Influence of Spatial Rainfall Gradients on River Longitudinal Profiles and the Topographic Expression of Spatio-temporally Variable Climate in Mountain Landscapes

Joel S Leonard[1] and Kelin X Whipple[1]

[1]Arizona State University

November 30, 2022

Abstract

Mountain landscapes have dynamic climates that, together with tectonic processes, importantly influence their topographic evolution. While spatio-temporal changes in rainfall are ubiquitous in these settings, their influence on river incision has been little studied. Here, we investigate how changes in rainfall pattern should affect both the steady state form and transient evolution of river profiles at the catchment scale using the stream power model. We find that non-uniform rainfall patterns complicate steady state relationships among conventional catchment-wide metrics like mean rainfall, channel steepness, and fluvial relief, which can influence the apparent sensitivity of landscapes and erosion rates to rainfall variations. We also find that transient responses to changes in rainfall pattern have an inherently multi-stage nature that importantly differs from expected responses to uniform changes in rainfall. This has several important implications, specifically for detecting transient responses to changes in rainfall pattern (and more broadly climate) in natural settings, and for interpretations of landscape morphometrics above and below transient knickpoints. We find that disparate responses by rivers and river segments that experience different rainfall conditions, particularly trunk and tributary rivers, are an important factor in understanding catchment-wide responses, and accounting for such disparities may be important for detecting and quantifying landscape sensitivity to rainfall variations. Lastly, we show how explicitly accounting for rainfall patterns in channel steepness calculations, and thus variations in erosional efficiency, may be a necessary step toward overcoming challenges related to rainfall variations, and thus ultimately for advancing understanding of landscape sensitivity to climate in mountain settings.

Hosted file

`supporting information.docx` available at https://authorea.com/users/561680/articles/609014-influence-of-spatial-rainfall-gradients-on-river-longitudinal-profiles-and-the-topographic-expression-of-spatio-temporally-variable-climate-in-mountain-landscapes

Influence of Spatial Rainfall Gradients on River Longitudinal Profiles and the Topographic Expression of Spatio-temporally Variable Climate in Mountain Landscapes

Joel S. Leonard[1] and Kelin X. Whipple[1]

[1]School of Earth and Space Exploration, Arizona State University, Tempe, Arizona, USA

Corresponding Author: Joel S. Leonard (joel.leonard@asu.edu)

Key Points

- Spatially variable rainfall complicates steady state relationships between mean rainfall and conventional topographic and erosion metrics.
- Transient responses to changes in rainfall pattern differ from uniform changes in rainfall, which affects how they may be detected.
- Rainfall gradients can obscure the sensitivity of fluvial erosion to rainfall variations and impede quantification of climate sensitivity.

Abstract

Mountain landscapes have dynamic climates that, together with tectonic processes, importantly influence their topographic evolution. While spatio-temporal changes in rainfall are ubiquitous in these settings, their influence on river incision has been little studied. Here, we investigate how changes in rainfall pattern should affect both the steady state form and transient evolution of river profiles at the catchment scale using the stream power model. We find that non-uniform rainfall patterns complicate steady state relationships among conventional catchment-wide metrics like mean rainfall, channel steepness, and fluvial relief, which can influence the apparent sensitivity of landscapes and erosion rates to rainfall variations. We also find that transient responses to changes in rainfall pattern have an inherently multi-stage nature that importantly differs from expected responses to uniform changes in rainfall. This has several important implications, specifically for detecting transient responses to changes in rainfall pattern (and more broadly climate) in natural settings, and for interpretations of landscape morphometrics above

28   and below transient knickpoints. We find that disparate responses by rivers and river segments that

29   experience different rainfall conditions, particularly trunk and tributary rivers, are an important factor in

30   understanding catchment-wide responses, and accounting for such disparities may be important for

31   detecting and quantifying landscape sensitivity to rainfall variations. Lastly, we show how explicitly

32   accounting for rainfall patterns in channel steepness calculations, and thus variations in erosional

33   efficiency, may be a necessary step toward overcoming challenges related to rainfall variations, and thus

34   ultimately for advancing understanding of landscape sensitivity to climate in mountain settings.

35   **Plain Language Summary**

36   Mountain landscapes typically experience different amounts of rainfall with increasing elevation. It is

37   widely thought that such differences should have a fundamental role in controlling the efficiency of

38   erosional processes. This is particularly true for river erosion, which is the dominant erosional process

39   shaping topography of most unglaciated mountain landscapes, because their erosive power is related to

40   the amount and rate of discharge. However, much of our understanding about how rainfall influences the

41   efficiency of river erosion, and how rivers adjust their form to accommodate changes in rainfall as climate

42   changes with time, is based in a framework that compares the effects of different amounts rainfall. This

43   framework typically assumes rainfall is uniformly distributed in the river basin, and therefore neglects the

44   influence of spatially variable rainfall that mountain rivers typically experience. We find that even modest

45   along-stream variations in rainfall can complicate common expectations about how topography should

46   reflect differences in rainfall. Expectations about how rivers adjust to changes in rainfall pattern, and

47   more broadly to changes in climate, are similarly affected. These findings have important implications for

48   recognizing both the influence of modern spatial variations in climate on active landscape processes and

49   ongoing adjustments to past climate changes.

50   **1. Introduction**

51   **1.1 Motivation**

52   Advances in tectonic geomorphology require quantitative understanding about relationships among

53   climate, tectonics, and erosion. In temperate mountain landscapes, studies of bedrock rivers provide

54   important insights into interactions between these processes (e.g., D'Arcy & Whittaker, 2014; Harel et al.,

55   2016; Kirby & Whipple, 2012; Lague, 2014; Olen et al., 2016; Scherler et al., 2017; Kelin X Whipple &

56   Tucker, 1999; Whittaker, 2012). However, despite longstanding theoretical support for the notion that

57   climate, like tectonics, has a fundamental role influencing erosion (e.g., Bonnet & Crave, 2003; Howard

58   & Kerby, 1983; Lague, 2014; Molnar, 2001; Perron, 2017; Rinaldo et al., 1995; Tucker & Slingerland,

59   1997), a direct, general relationship between climate and erosion has proven elusive (Perron, 2017;

60   Whittaker, 2012). In this paper, we explore the extent to which this conundrum may reflect limitations in

61   the current framework describing how climate-related signals should be expressed in landscapes that, in

62   turn, may impede recognition of diagnostic characteristics of landscape response to climate change.

63   Orographic precipitation patterns are ubiquitous in mountain landscapes. In general, they develop from

64   the interaction of humid air masses with topographic relief (see Roe, 2005 for an overview), and can

65   create dramatic spatial and elevation dependent gradients in precipitation. While numerous factors affect

66   orographic precipitation patterns in detail, broadly speaking, atmospheric moisture content and

67   topographic characteristics (e.g., relief) are primary physical controls on their development (e.g., Held &

68   Soden, 2006; Roe, 2005; Roe et al., 2008; Trenberth et al., 2003). Because atmospheric moisture content

69   depends strongly on temperature (i.e., Clausius-Clapeyron relationship; Held & Soden, 2006; Roe, 2005;

70   Trenberth et al., 2003), shifts in temperature that accompany changes in climate must influence these

71   precipitation patterns. Therefore, if erosional processes in these landscapes are generally sensitive to

72   variations in precipitation, then changing characteristics of orographic precipitation patterns (e.g., strength

73   of rainfall gradients) with changes in climate should importantly influence mountain landscape evolution.

74   In mountainous settings, transverse rivers tend to cross orographic precipitation gradients, which are

75   generally oriented orthogonally to the topographic trend of the range. Their tributaries, on the other hand,

76   typically experience a relatively muted range in precipitation due to their orientation and/or smaller areal

77   extent. Consequently, rivers of different size, orientation, and position often experience dramatically

78   different precipitation conditions. Within large river basins, these differences may be substantial.

79   Exposure to orographic precipitation patterns is expected to systematically affect river profile concavity;

80   increases in precipitation with distance upstream lowers profile concavity, while the opposite trend

81   increases profile concavity (Han et al., 2014, 2015; Roe et al., 2002, 2003; Ward & Galewsky, 2014).

82   Importantly, this implies that adjustment to a change in orographic precipitation pattern should involve

83   longitudinally variable amounts of incision (i.e., transient changes in concavity). Furthermore, because

84   transverse rivers set erosional base level for their tributaries, any along-stream variation in incision

85   exhibited by transverse rivers as they adjust will necessarily drive spatially and temporally variable base

86   level histories for tributaries. Developing a framework that accommodates such variability and its

87   influence on river profile evolution is a fundamental need.

88   **1.2 Approach and Scope**

89   In this paper, we investigate how spatio-temporal changes in precipitation may influence erosion and

90   topography of mountain landscapes using the stream power model (SPM). First, we show how simple

91   spatial gradients in rainfall, resembling typical orographic rainfall gradients (i.e., increasing or decreasing

92   downstream; herein referred to as bottom-heavy, and top-heavy, respectively), influence river profile

93   form at steady state in one dimension. Then, we present a sensitivity analysis that characterizes how

94   changes in rainfall pattern should affect the steady-state form of a given river profile. Following this, we

95   use a quasi-two-dimensional numerical model to simulate the response of a transverse, trellised river

96   network to a change in rainfall pattern, which we compare to better-understood spatially uniform changes

97   in rainfall. Finally, we discuss some implications of these results for studies set in mountain landscapes. A

98   comprehensive analysis of the co-evolution of orographic rainfall patterns and topography is beyond the

99   scope of this paper. Instead, we focus on characterizing the controls on landscape response to imposed

100   changes in rainfall patterns, highlighting where expectations differ from uniform changes in rainfall, and

101   implications of those differences.

102   **2. Methods**

103   **2.1 Model Description**

104   Following Riihimaki et al., (2007), we use a quasi-two-dimensional finite difference model of bedrock

105   channels to represent an idealized river basin. We abstract river basin topology to comprise a single one-

106   dimensional trunk profile and 51 regularly spaced (1 km) one-dimensional tributary profiles. We model

107   erosion as detachment-limited (Howard, 1994; Whipple & Tucker, 1999) following a general form of the

108   SPM:

109   $$E = KA^mS^n, \tag{1a}$$

110   $$K = K_p\bar{P}^m, \tag{1b}$$

111   $$E = K_pQ^mS^n, \tag{1c}$$

112   where E is the erosion rate, K and K_p are erosional efficiency constants, A is upstream drainage area, S is

113   the channel slope, $\bar{P}$ is the upstream average rainfall rate, Q is water discharge equal to $\bar{P}A$, and m and n

114   are positive constant exponents (Table 1). We use $n = 2$ and $m = 1$ for all model runs as values of $n > 1$

115   appear more appropriate in many settings (e.g., Adams et al., 2020; Harel et al., 2016; Lague, 2014).

116   First-order results do not rely on choices of m or n providing the ratio between the two is maintained, but

117   the nonlinear dependence of erosion rate on slope (i.e., $n = 2$) affects details of the transient behavior, and

118   because $m = 1$, note that K is directly proportional to both $\bar{P}$ and Q. We explicitly treat the influence of

119   climate on erosional efficiency (e.g., Adams et al., 2020; Roe et al., 2003) such that K_p is independent of

120   rainfall, but still encapsulates a number of factors including rock properties and details of erosional

121   processes (Royden & Perron, 2013; Whipple & Tucker, 1999). Rock uplift rate (U) and K_p are spatially

122   and temporally uniform for the duration each model run, and invariant across model runs. We define

123   drainage area (A) for both the trunk and tributary profiles following Hack, (1957):

$$A = k_a x^h + A_c, \tag{2}$$

125   where x is distance along the channel downstream from the channel head, k_a and h are constants, and A_c is

126   the upstream drainage area at the channel head – equal to 1 km^2. Channel length (L) and drainage area are

127   fixed for each profile, and do not evolve over the course of a model run (Table 1). Discharge (Q) is

128   calculated at each profile node from equation (2) as:

$$Q = \overline{P}A. \tag{3}$$

130   This definition assumes the simplest hydrological condition where all rainfall is converted directly to

131   runoff. Discharge does not pass from tributaries to the trunk river as drainage area along the trunk is set

132   by equation (2) independently. This approach allows closely spaced tributaries with uniform

133   characteristics to better describe erosional response while maintaining empirically supported scaling

134   between channel length and drainage area throughout the modelled river basin. Tributary outlets are fixed

135   to the elevation of the trunk profile at their confluence. Importantly, this means that while there is not

136   two-dimensional hydrological coupling through discharge, transient signals are communicated from the

137   trunk to tributaries through variations in base level.

138   The initial condition for all models is steady state with spatially uniform rainfall. For simplicity, we

139   model orographic precipitation exclusively as constant gradients in rainfall (i.e., linear changes with

140   distance) that span the length of the trunk river (and orthogonal to tributaries). Imposed changes in

141   rainfall evolve linearly over the first 10 kyr of model time. Tributary profiles are modeled with spatially

142   uniform rainfall set by their position along the trunk profile; thus, individual tributaries experience

143   spatially uniform changes in rainfall as orographic gradients evolve. This simplification is consistent with

144   the notion that, due to their smaller areal extent and orientation, tributaries set within mountain-belt scale

145   orographic gradients experience relatively uniform rainfall.

146   **2.2 Analysis of River Profiles and Erosion Rates**

147   We quantify river profile form and responses to changes in rainfall patterns using channel steepness

148   metrics and erosion rates. These metrics are commonly used, and often in tandem, to study influences of

149   climate and/or tectonics in mountain settings (Adams et al., 2020; Bookhagen & Strecker, 2012; Cyr et

150   al., 2014; DiBiase et al., 2010; Duvall, 2004; Godard et al., 2014; Insel et al., 2010; Kober et al., 2015;

151   Morell et al., 2015; Olen et al., 2016; Ouimet et al., 2009; Portenga et al., 2015; Safran et al., 2005;

152   Scherler et al., 2014; Vanacker et al., 2015; Willenbring et al., 2013).

153   Within the SPM framework, river slope is directly related to its erosional capacity (Equations 1a, 1c). A

154   frequently applied metric in mountain landscapes that accounts for the general covariation between slope

155   and drainage area is a normalized channel steepness index, k_{sn}:

156
$$k_{sn} = SA^{\theta_{ref}}, \tag{4}$$

157   where θ_{ref} is the reference concavity index (Wobus et al., 2006). We use a value of $\theta_{ref} = 0.5$, which is

158   consistent with common usage in natural landscapes and with SPM predictions that $\theta_{ref} = m/n \approx 0.5$ where

159   rock uplift rate (U) and erosional efficiency (K) are uniform (Tucker & Whipple, 2002). As previously

160   noted, the SPM predicts that orographic rainfall gradients should produce longitudinal variations K

161   (Equation 1b) that, in turn, affect the concavity index, θ (Han et al., 2014, 2015; Roe et al., 2002, 2003).

162   Any such variations are systematically reflected in the spatial pattern of k_{sn} and $\theta \neq \theta_{ref}$ is expected.

163   Importantly, however, many studies relate upstream-average values of k_{sn} to measured spatially-averaged

164   erosion rates, which relies on quasi-uniform (or linear) upstream k_{sn} to be valid (Wobus et al., 2006).

165   Therefore, in cases where systematic longitudinal variations in K affect the downstream pattern of k_{sn} (i.e.,

166   upstream k_{sn} varies non-linearly), the meaning of such an average is not obvious.

167   To address complications introduced by rainfall gradients, we use discharge rather than drainage area to

168   calculate channel steepness to arrive at k_{sn-q} (Adams et al., 2020):

169
$$k_{sn-q} = SQ^{\theta_{ref}}. \tag{5}$$

170   We note, k_{sn-q}, like k_{sn}, is an empirically supported metric independent from the SPM. In principle,

171   however, k_{sn-q} is analogous to Erosion Index (EI) used by Finlayson et al., (2002) provided that $m/n \approx \theta_{ref}$,

172   such that $EI = (k_{sn-q})^n$. Importantly, to the extent that the SPM captures the influence of discharge on

173   erosional efficiency, it predicts that along-stream variations in k_{sn-q} should scale with local erosion rate,

174   much like it does for k_{sn} where K is spatially uniform. Hereafter, we use k_{sn} and k_{sn-q} to refer to upstream

175   averaged values, consistent with their common usage in analyses of catchment-mean erosion rates, unless

176   we specifically state that they represent local values.

177   Millennial-scale catchment-averaged erosion rates measured, for example, using cosmogenically-derived

178   [10]Be found in quartz in alluvial sediment (e.g. Bierman & Steig, 1996; Brown et al., 1995; Granger et al.,

179   1996), seek to quantify erosion rates at the river basin scale. At steady state, spatially-averaged erosion

180   rate, local incision rate, and rock uplift rate are equivalent; however, during periods of transient

181   adjustment these values differ, complicating interpretations (Willenbring et al., 2013; Wobus et al., 2006).

182   To make our results more portable to studies of natural landscapes, we calculate the spatially averaged

183   erosion rate (E_{avg}) in addition to the instantaneous vertical incision rate (E):

$$E_{avg\,j} = \left(\sum_{x_h}^{j} [E_j \cdot (A_j - A_{j-1})] \right) / A_j, \tag{6}$$

185   where j corresponds to a downstream node of the profile, and x_h is the channel head.

3. 1-Dimensional Profiles

3.1 Influence of Longitudinal Rainfall Gradients on River Profiles at Steady State

188   Where rainfall is spatially uniform, topographic metrics (e.g., fluvial relief, channel steepness) are

189   expected to vary inversely and monotonically with mean rainfall at steady state, but non-uniform rainfall

190   patterns complicate these expectations. Steady state river profiles subjected to varying amounts of

191   spatially uniform rainfall are shown in Figure 1a alongside discharge (Q) as a function of distance

192   downstream for each profile, and corresponding relationships between mean rainfall ($\overline{P}$) and fluvial relief

193   (R), k_{sn}, and k_{sn-q}. In comparison, Figure 1b shows a comparable suite of model steady state profiles

194   subject to uniform, decreasing upstream, and increasing upstream rainfall patterns, that constitute an

195   example where fluvial relief and k_{sn} actually increase with mean rainfall. This reversal reflects limitations

196   of metrics like mean rainfall and k_{sn} where climate is spatially variable.

197   Systematic longitudinal variations in rainfall require that the mean (upstream average) rainfall values

198   change systematically downstream, which in turn influences erosional efficiency (K) in a similarly

199   systematic manner (Equation 1b), and thus equilibrium channel slope. Where such spatial variations exist,

200   mean values of rainfall and k_{sn} therefore depend on where they are measured, which makes the meaning

201   of a given value difficult to interpret. In contrast, to the extent that the SPM captures the influence of

202   discharge on erosional efficiency, k_{sn-q} is independent of changes in mean rainfall, as is shown in Figure 1.

203   Comparison of SPM equations for k_{sn} and k_{sn-q} at steady state ($E = U$) clearly shows this difference:

$$k_{sn} = \left(\frac{U}{K_p \overline{P}^m} \right)^{1/n}, \tag{7a}$$

205
$$k_{sn-q} = \left(\frac{U}{K_p}\right)^{1/n}.$$
(7b)

206 For spatially uniform rock uplift rate (U) and K_p, steady state fluvial relief (R) is proportional to the
207 upstream integrated discharge (Han et al., 2015; Roe et al., 2003; Royden & Perron, 2013). Integrating
208 equation (1c) from base level (x_b) upstream to the channel head (x_h), it can be shown that:

209
$$R = \left(\frac{U}{K_p}\right)^{1/n} \int_{x_b}^{x_h} Q^{-m/n} \, dx.$$
(8)

210 We point out that because fluvial relief depends on the cumulative effect of discharge (Q) it does not
211 necessarily scale monotonically with discharge or rainfall measured at any single position, or averaged
212 along any segment of a profile, except under the special condition where rainfall is spatially uniform
213 (Gasparini & Whipple, 2014; Han et al., 2015). This alone suggests that quantifying the magnitude of
214 temporal changes in mean rainfall (e.g., degree to which mean rainfall increases or decreases) is
215 inadequate, at least under some conditions, to predict morphological responses of mountain landscapes to
216 changing climate, or how a transient response may be expressed. Instead, how rainfall patterns have
217 changed, and specifically, *where* rainfall has changed within a given catchment must be considered.

3.2 Transient River Profile Response to Spatio-temporal Changes in Rainfall Patterns

219 According to the SPM, transient responses to climate change are primarily driven by changes in discharge
220 that, in turn, affect erosional efficiency. As orographic precipitation patterns change with changes in
221 climate, different positions within a river basin may experience an increase or a decrease in rainfall. This
222 spatial rainfall variability fundamentally affects how discharge accumulates, and ultimately how river
223 profiles respond during transient adjustment.

224 Whether discharge locally increases or decreases following a change in rainfall pattern depends on how
225 the rainfall pattern has changed upstream from a given position. (Hereafter we use subscripts i and f,
226 respectively, to denote initial and final steady states, before and after a change in rainfall pattern.) As with
227 spatially uniform changes in rainfall, local equilibrium channel slope varies inversely with discharge.
228 While discharge is somewhat buffered from localized variations in rainfall by integrating upstream
229 conditions, because discharge accumulates non-linearly downstream relatively modest rainfall gradients
230 can have a strong influence on the downstream pattern. Notably, we find that a wide range of changes in
231 rainfall patterns cause inversions in relative changes in discharge along a river. That is, while discharge
232 may increase in upstream locations ($Q_f > Q_i$) for a given change in rainfall pattern, it may also decrease in

233   downstream locations ($Q_f < Q_i$), or vice versa.

234   Along-stream reversals in the relative change in discharge imply a position where discharge, and
235   therefore also equilibrium slope, are unchanged ($Q_f = Q_i$ and $S_f = S_i$). We refer to this position as x_{sc}, and
236   as we will show, changes in rainfall pattern that cause such reversals drive unique transient adjustments.
237   For now, we note that upstream of x_{sc} initial and final steady state profiles begin to converge (see Figure
238   2). Thus, x_{sc} marks a local maximum difference between initial and final steady state profiles. This
239   convergent behavior contrasts with expectations for spatially uniform changes in rainfall where the
240   difference in channel bed elevation increases monotonically upstream from the outlet (Figure 1a).

241   Assuming spatially uniform rock uplift rate (U) and K_p, the magnitude of this difference along the profile
242   between initial and final states, Δz_{Sc}, can be expressed:

$$\Delta z_{Sc} = \left(\frac{U}{K_p}\right)^{1/n} \int_{x_b}^{x_{sc}} (Q_f - Q_i)^{-m/n} \, dx. \qquad (9)$$

244   In some circumstances, initial and final steady state profiles can intersect. The condition that determines
245   whether this occurs can be similarly expressed:

246

$$0 = \left(\frac{U}{K_p}\right)^{1/n} \int_{x_b}^{x_{zc}} (Q_f - Q_i)^{-m/n} \, dx, \qquad (10)$$

248   where x_{zc} is the position of intersection (Figure 2). Interestingly, x_{zc} marks a change in the net adjustment
249   required to reach steady state (i.e., enhanced incision vs. surface uplift). Also, rainfall patterns that satisfy
250   this condition are those that lead to positive relationships between mean rainfall and fluvial relief (Figure
251   1b). That is, these are changes in rainfall pattern where the SPM predicts an increase in mean rainfall
252   would actually support growth of catchment topographic relief rather than a reduction, and vice versa.

253   **3.3 Sensitivity Analysis of 1-D River Profiles to Spatio-temporal Changes in Rainfall Patterns**

254   In this section, we present a sensitivity analysis to evaluate the influence of changes in rainfall pattern on
255   discharge and fluvial relief compared to uniform changes in rainfall by exploring how different rainfall
256   gradients should affect a given steady state river profile (Figure 3).

257   We define different fields bounding rainfall gradients that result in different classes of behavior (Figure

258   3a). Boundaries demarcating these fields are independent of U, K_p, m, and n provided m/n is unchanged.

259   Channel length has a negligible influence for channels longer than a few kilometers where $A \gg A_c$. The h

260   exponent in Hack's relationship (Equation 2) can influence field boundaries, as indicated in Figure 3a;

261   however, the effect is minor for the range of h values typically observed in nature (e.g., Rigon et al.,

262   1996). Contours of Q_f/Q_i illustrate the extent to which a given rainfall gradient represents a net wetter (Q_f

263    $/Q_i > 1$) or drier ($Q_f/Q_i < 1$) condition (Figure 3b). Contours of R_f/R_i describe the extent to which fluvial

264   relief increases ($R_f/R_i > 1$) or decreases ($R_f/R_i < 1$). These contours show that steady state fluvial relief (R_f

265    $/R_i$) is sensibly correlated with mean rainfall (Q_f/Q_i), but the relationship is complex when rainfall is not

266   spatially uniform.

267   White fields (Figure 3, both panels) encompass rainfall gradients – and uniform changes in rainfall –

268   where the entire profile would experience wetter or drier conditions. Transient adjustments to such

269   gradients generally mimic adjustments to spatially uniform increases or decreases in rainfall, although

270   non-uniform changes are expected to affect adjustments differently than uniform changes in detail.

271   Light grey fields (Figure 3a) encompass rainfall gradients that would produce x_{sc}, but not x_{zc}; thus, relative

272   changes in discharge and equilibrium slope would invert along the profile, but initial and final steady state

273   profiles would not intersect. During transient adjustment, the mode of transient adjustment is variable in

274   space and time upstream of x_{sc} (variably $E > U$ or $E < U$; Figure 2). Despite this, the net change in fluvial

275   relief caused by these changes is inversely related to the change in mean rainfall at steady state, consistent

276   with expectations for spatially uniform changes in rainfall. Lastly, x_{sc} marks the position of the absolute

277   maximum difference between initial and final steady states in these cases, not the channel head.

278   Therefore, while the entire profile experiences net incision or surface uplift to reach steady state, the

279   largest changes are along the central part of the profile.

280   Dark grey fields (Figure 3a) encompass rainfall gradients that produce both x_{sc} and x_{zc} and are

281   characterized by the most complex transient responses. Implied relative differences in discharge and slope

282   follow as for light grey fields, and modes of transient adjustment are similarly spatio-temporally variable

283   upstream from x_{sc} (Figure 2). The distinguishing feature of these gradients is that the resulting steady state

284   fluvial relief is positively related to the change in mean rainfall (e.g., Figures 1b, 2). The absolute

285   maximum difference between initial and final steady states may either be at x_{sc} or at the channel head in

286   these cases depending on specific characteristics of the change in rainfall gradient.

287   This analysis reveals several interesting ways that changes in rainfall pattern influence river profiles

288   differently than expected for uniform changes. First, changes in longitudinal rainfall gradients that result

289   in complex transient responses (grey fields in Figure 3a) appear relatively common and do not require

290   extreme changes in rainfall patterns. Note, we define our usage of 'complex transient responses' hereafter

291   to include all responses that result in x_{sc} (i.e., both grey fields in Figure 3a), unless we specify otherwise.

292   That these complex responses arise readily from a range of changes in rainfall patterns suggests that these

293   types of responses may be a typical aspect of landscape evolution in mountain settings.

294   Our analysis also shows that among changes in rainfall pattern where a positive relationship between the

295   change in mean rainfall and fluvial relief is expected (dark grey fields in Figure 3a), changes to top-heavy

296   and bottom-heavy conditions have an asymmetric influence on fluvial relief. While top-heavy gradients in

297   this category always inhibit growth of fluvial relief (R_f /R_i always < 1) and bottom-heavy gradients

298   promote topographic growth, contour spacing of changes in fluvial relief show that incremental changes

299   in bottom-heavy gradients have a stronger influence (Figure 3). This asymmetry follows directly from

300   equation 8, and arises because higher rainfall in the headwaters of a catchment (top-heavy) influences

301   equilibrium channel slope everywhere downstream, but higher rainfall near base level (bottom-heavy)

302   does not influence channel slope upstream.

303   Testing a broad range of parameters that may be applicable to major mountain ranges (e.g., K_p, U, h, L),

304   we find that changes in rainfall gradients alone may support increases or decreases in steady state fluvial

305   relief by as much as 10^2–10^3 m in the opposite direction expected based on the change in mean rainfall

306   assuming a uniform change (e.g., an increase in relief associated with an increase in mean rainfall).

307   Simultaneously, the same change may drive as much as 10^1–10^2 m of enhanced incision or surface uplift

308   along downstream and central portions of catchments consistent with conventional expectations for the

309   change in mean rainfall. This spatially segregated behavior may be particularly important for

310   understanding sediment transport out of mountain catchments and signals related to development of

311   landforms like fluvial terraces, for example, which we do not treat in this paper but nevertheless warrants

312   further research.

313   Lastly, we emphasize that the response to a change in rainfall pattern strongly depends on the initial

314   conditions – we revisit this point in section 5.1. Together this analysis supports the notion that non-

315   uniform changes in rainfall pattern can readily and importantly influence landscape form and processes in

316   ways that fundamentally differ from expectations for spatially uniform changes in rainfall.

317   **4. Transient Evolution of River Basins Responding to Changes in Rainfall Patterns**

318   The transient response of a river basin to a change in rainfall pattern is highly dynamic. Fortunately, many

319   of the ideas laid out above for 1-dimensional profiles intuitively transfer to understanding how signals

320   propagate through a simple trellis drainage network, albeit with some additional considerations. It is

321   important to remember that trunk (transverse) rivers control base level for tributaries. Complex responses

322   to changing rainfall patterns, like those described above where both the magnitude and mode of transient

323   adjustment vary along the trunk profile in space and time, necessarily result in varying boundary

324   conditions for tributaries. In addition, tributary responses to these variable base level signals are

325   modulated by the rainfall history experienced by a given tributary, which is always different from the

326   trunk. Finally, adjustments migrate upstream at a finite rate, so there is a time lag between a change in

327   rainfall pattern and arrival of the associated base level signals from the trunk adjustment to a given

328   tributary. The duration of this lag, as well as local rainfall conditions within a tributary catchment, are a

329   function of its position along the trunk profile.

330   In the following, we explore the transient response of modelled trellis river basins to four representative

331   climate change scenarios: (1) a spatially uniform decrease in rainfall, (2) a spatially uniform increase in

332   rainfall, (3) a shift from spatially uniform rainfall to a bottom-heavy rainfall gradient, and (4) a shift from

333   spatially uniform rainfall to a top-heavy rainfall gradient.

4.1 Case 1: Spatially Uniform Decrease in Rainfall

334

335   The modelled catchment response to a spatially uniform decrease in rainfall is characterized by

336   adjustment to uniformly higher k_{sn} and an increase in steady state fluvial relief. For this model run,

337   rainfall is decreased from 2 to 1 m/yr, causing discharge to decrease similarly by 50% (Movie S1).

338   We observe an effectively instantaneous transient decrease in erosion rate across the entire channel

339   network driven by a decrease in erosional efficiency directly proportional in magnitude to the change (i.e.,

340   50%; recall $m = 1$). The resulting disequilibrium, with $E < U$, drives surface uplift and upstream migration

341   of a convex-up slope-break knickpoint, and eventually a ~40% increase in fluvial relief. This change in

342   erosional efficiency differently affects k_{sn} and k_{sn-q} (Figure 4).

343   In k_{sn}–E_{avg} space (Figure 4a), the change rainfall causes the trunk river and tributary network to shift

344   uniformly onto a different erosional efficiency curve that describes the expected relationship between k_{sn}

345   and erosion rate for a given erosional efficiency at steady state. Specifically, both shift from $K=2 \cdot K_p$ to

346   $K=K_p$ ($K_f = 0.5 \cdot K_i$); thus, everywhere exhibits 50% lower erosional efficiency. Following this initial shift,

347   the trunk river and individual tributaries approximately follow this new curve during adjustment toward

348   higher erosion rates and k_{sn} to return to steady state, although in detail they deviate and exhibit a concave-

349   up trajectory. This deviation is a result of averaging segments above and below the migrating knickpoint

350   into mean (upstream-averaged) k_{sn} and erosion rate values.

351   In $k_{sn\text{-}q}$–E_{avg} space (Figure 4b), both the initial and final steady state conditions plot in the same location

352   on the curve for $K=K_p$. The initial decrease in erosional efficiency causes the trunk and tributaries to shift

353   uniformly along this curve to lower $k_{sn\text{-}q}$ and erosion rate rather than shifting onto a different curve.

354   During adjustment both generally follow this curve to return to steady state, minor transient deviations as

355   seen for k_{sn} notwithstanding.

4.2 Case 2: Spatially Uniform Increase in Rainfall

357   The modelled catchment response to a spatially uniform increase in rainfall is characterized by adjustment

358   to uniformly lower k_{sn} and a decrease in steady state fluvial relief. To compare responses, we invert the

359   change in rainfall from the previous example, and rainfall is increased from 1 to 2 m/yr, which results in a

360   100% increase in discharge (Movie S2).

361   We observe a broadly symmetrical response to Case 1, where the twofold increase in rainfall leads to an

362   initial twofold increase in erosion rate ($E > U$) and a ~30% decrease in steady state fluvial relief. The

363   transient knickpoint is concave-up, but as it migrates upstream it relaxes and broadens, as is expected for

364   a concave-up knickpoints where n > 1 (Royden & Perron, 2013). The signal of transient adjustment

365   communicated to tributaries is consequently protracted, making morphological adjustments more diffuse

366   in nature.

367   Responses reflected in k_{sn}–E_{avg} and $k_{sn\text{-}q}$–E_{avg} relationships also mirror Case 1. As is characteristic for k_{sn},

368   the initial change in erosional efficiency causes the trunk and tributary network to shift onto a different

369   steady state erosional efficiency curve; in this case, from $K = K_p$ to $K = 2 \cdot K_p$, and they generally follow

370   this curve during adjustment (Figure 4a). Minor deviations from this curve exhibit a convex-up pattern

371   (inverted from Case 1) due to the opposite knickpoint shape in this case (concave vs. convex). Meanwhile

372   in $k_{sn\text{-}q}$–E_{avg} space (Figure 4b), the initial and final steady state conditions for both the trunk and tributary

373   network plot in the same location, as in Case 1. The change in rainfall again causes a shift only along the

374    $K=K_p$ curve, but to uniformly higher $k_{sn\text{-}q}$ and erosion rate in this case, and they generally follow this

375   curve during adjustment back to steady state.

4.3 Case 3: Spatially Uniform to Bottom-heavy (Overall Wetter Climate)

377   In this scenario, we model the catchment response to a change in rainfall pattern from spatially uniform

378   1.5 m/yr to a gradient that decreases upstream from 4 to 0.5 m/yr, which results a complex transient

379   response. This change results in a nearly 80% increase in mean rainfall to ~2.7 m/yr, but also remarkably

380   drives a 30% increase in fluvial relief (Figure 3b; Movie S3). Importantly, this contrasts with the 25%

381   decrease in fluvial relief expected for a spatially uniform increase in mean rainfall of the same magnitude.

382   *4.3.1 Case 3: Trunk Response*

383   In this case, because the change in rainfall is variable along the trunk river, the initial change in erosion

384   rate is also variable. The trunk river experiences an approximately 80% increase in erosion rate at the

385   outlet ($E > U$), and a decrease of 67% in the headwaters ($E < U$), corresponding to the change in

386   upstream average rainfall along its length. At x_{sc} (located ~27 km upstream from the outlet), $Q_f = Q_i$, $S_f =$

387   S_i, and so immediately following the change in rainfall $E = U$ holds true; thus, no change in erosion rate

388   occurs initially at x_{sc}. Increased erosion rate at the outlet produces a concave-up knickpoint; however, as

389   the knickpoint migrates upstream it progressively sharpens and eventually evolves into an oversteepened

390   convex-up knickpoint. Oversteepening is a consequence of the upstream decrease in erosional efficiency

391   driven by the rainfall gradient that is exacerbated by, but does not depend on, differing modes of

392   adjustment upstream and downstream of x_{sc} related to the complex response. This is analogous to

393   knickpoint behavior described by Forte et al. (2016) and Darling et al. (2020) where modelled lithologic

394   contacts demarcate similar relative variations in erosional efficiency (i.e. hard rocks over soft rocks).

395   Lastly, we note that everywhere upstream of x_{sc} over-adjusts during transient adjustment leading to

396   variable modes of adjustment in time as well as in space, which is a characteristic of complex responses

397   in general. The overadjustment we observe is essentially the whiplash response described by Gasparini et

398   al. (2006, 2007), but notably results here without sediment flux. This continuous evolution of the trunk

399   knickpoint has important consequences for signals passed to tributaries.

400   *4.3.2 Case 3: Tributary Response*

401   Tributary responses to the change rainfall pattern depend largely on their position. Collectively, the

402   network of tributaries experiences the full range of the rainfall gradient (i.e., 4 to 0.5 m/yr), and individual

403   tributaries experience changes in erosional efficiency proportional to the change in rainfall that they

404   experience. Notably, the change in rainfall and erosional efficiency experienced by a given tributary is

405   always different from the trunk river at their confluence (Figure 2 inset). Additionally, tributaries also

406   respond to changing boundary conditions related to continuous adjustment of the trunk river. These

407   signals are often conflicting. For example, in this scenario, enhanced incision during the initial transient

408   response of the trunk river causes tributaries in downstream locations ($x < x_{sc}$) to experience a relative

409   increase in the rate of base-level fall. Alone, this should promote profile steepening, but higher erosional

410   efficiency due to higher rainfall in these tributaries counteracts steepening. The net effect of this

411   competition plays out differently as a function of tributary position throughout the transient evolution

412   (i.e., space and time) as 1) the discrepancy between the local rainfall conditions experienced by tributaries

413   and the upstream averaged rainfall experienced by the trunk profile narrows upstream (Figure 2 inset), 2)

414   the transient base level signal (i.e., trunk knickpoint) changes shape as it sweeps upstream, and 3) the

415   duration of transient adjustment increases upstream.

416   *4.3.3 Case 3: k_{sn}–E_{avg} and k_{sn-q}–E_{avg}*

417   Plots of k_{sn}–E_{avg} and k_{sn-q}–E_{avg} clarify some additional features of the dynamic transient response to

418   spatially variable rainfall as it sweeps through different parts of the catchment (Figure 5). We note that the

419   trunk profile exhibits higher k_{sn} and k_{sn-q} values and spans a relatively narrower range in erosion rates than

420   tributaries during transient adjustment, reflecting the fundamentally different ways they experience the

421   modelled rainfall gradient. This suggests that the network of tributaries (isolated smaller catchments that

422   experience a range in rainfall) inherently incorporates a more direct signal of the change in rainfall

423   patterns compared to the trunk, which averages upstream rainfall variations – an important finding for

424   designing an effective sampling strategy in the field – discussed further in section 5.3.

425   In k_{sn}–E_{avg} space (Figures 5a, 5b), changes in erosional efficiency cause shifts onto curves for different

426   erosional efficiencies, as in Cases 1 & 2, but notably different positions along the trunk river and

427   individual tributary catchments shift by different amounts reflecting spatial variations in erosional

428   efficiency. The trunk profile response spans curves for $K = 0.5 \cdot K_p$ to ~$1.8 \cdot K_p$, while the network of

429   tributaries spans the range from curves for $K = 0.5 \cdot K_p$ to $4 \cdot K_p$. To first order, transient adjustment at a

430   given location for the trunk, or of a given tributary, moves it along these different curves toward steady

431   state as in Cases 1 & 2, but deviate in detail. As noted previously, positions upstream of x_{sc} over-adjust

432   before returning to steady state, which affects these general trajectories more than for uniform changes in

433   rainfall, exhibited by sharp inflections (Figure 5). Finally, we note that the final steady state condition for

434   both the trunk profile and network of tributaries encompasses a range of erosion efficiency values

435   (Figures 5a & 5b). Interestingly, for the trunk profile, the range of erosional efficiency values that

436   correspond to upstream mean k_{sn} values at steady state ($K = 0.5 \cdot K_p$ to ~$1.8 \cdot K_p$) are lower than that implied

437   by mean rainfall (i.e., $K = $~$2.7 \cdot K_p$; Figures 1b, 5a) – discussed further in section 5.2.

438   In k_{sn-q}–E_{avg} space (Figures 5c, 5d), differences between trunk and tributary responses and important

439   differences from k_{sn} are readily apparent. Initial and final steady state conditions plot in the same position,

440   as is characteristic of $k_{sn\text{-}q}$ because uplift rate is constant. Following the change in rainfall, the trunk

441   profile expands subparallel to the $K=K_p$ curve, where downstream locations are systematically shifted

442   toward higher erosional efficiency. This shift reflects systematic slope adjustments that must occur along

443   the trunk to bring it into equilibrium with the non-uniform rainfall pattern, and decreases with time as

444   morphological adjustments take place. Apart from this minor shift, different positions along the trunk

445   profile generally follow the $K=K_p$ curve during adjustment back to steady state. In tributaries, on the other

446   hand, the change in rainfall causes expansion precisely along the $K=K_p$ curve because they experience no

447   along-stream variations in rainfall. Tributaries again generally evolve along the $K=K_p$ curve toward

448   steady state (as with cases 1 and 2). Transient morphological adjustments affect this trajectory in detail

449   and deviations, which affect apparent erosional efficiency, are more significant in drier tributaries near the

450   headwaters. Overadjustment is also evident for both the trunk and tributaries, but because transient

451   evolution is generally along the steady state curve, it does not significantly affect the apparent erosional

452   efficiency. As a final note, we point out that dispersion around steady state erosional efficiency curve in

453    $k_{sn\text{-}q}$–E_{avg} space is minor over the entire course of the transient adjustment compared to dispersion in k_{sn}–

454   E_{avg} space – we expand on implications from this point in section 5.3.

455   **4.4 Case 4: Spatially Uniform to Top-heavy (Overall Drier Climate)**

456   In this final case, we the model the catchment response to a change in rainfall pattern from spatially

457   uniform 1.5 m/yr to a gradient that increases upstream from 0.25 to 2.25 m/yr, which also results a

458   complex transient response. This change results in a decrease in mean rainfall by 33% and a 10% decrease

459   in fluvial relief (Figure 3; Movie S4). Notably, this contrasts with a 22% increase in fluvial relief that

460   would be expected for a spatially uniform decrease in mean rainfall of the same magnitude.

461   *4.4.1 Case 4: Trunk Response*

462   In this case, the trunk river experiences a 33% initial decrease in erosional efficiency and erosion rate at

463   the outlet, and a 50% increase in the headwaters immediately following the change in rainfall pattern

464   (Figure 6). However, we note that this range is significantly narrower than the range of variations in

465   rainfall because of the buffering effect that concentrating rainfall in the headwaters has on downstream

466   changes in discharge (e.g., Figure 2 inset). Like Case 3, because this scenario also exhibits a complex

467   transient response, the transition between decreases in erosion rate downstream and increases upstream is

468   initially at position x_{sc}. Unlike Case 3, knickpoint shape does not invert during transient adjustment and is

469   always convex-up, although it does tend to relax downstream and sharpen upstream from x_{sc}, respectively.

470   Retention of the knickpoint shape is accommodated by over-adjustment upstream of x_{sc}, specifically by

471   progressively more rapid upstream adjustment (higher erosional efficiency) toward gentler slopes that

472   outpaces downstream adjustment. Because $E > U$ upstream of x_{sc}, over-adjustment of the profile promotes

473   incision below its steady state elevation and always adjusts to steady state from an understeepened

474   condition. Therefore, by the time that the migrating trunk knickpoint reaches positions upstream of x_{sc}, the

475   channel bed must uplift and the profile must steepen to achieve steady state, preserving the convex-up

476   knickpoint shape (Movie S4).

477   *4.4.2 Case 4 Tributary Response*

478   Complexities in the trunk response again dramatically affect the tributary responses, and generally mirror

479   complexities discussed in Case 3. Tributaries again respond to variable, and commonly, conflicting

480   signals. In this case, downstream of x_{sc}, tributaries initially respond to a decrease in rainfall (lower -

481   erosional efficiency) by steepening. However, along that same region the trunk profile experiences a

482   decrease in erosional efficiency that drives steepening and surface uplift, forcing tributaries to respond to

483   a conflicting signal of base-level rise (Movie S4). Additionally, as the network of tributaries experiences

484   the full range of the rainfall gradient – thus express a broader range in erosional efficiency – individual

485   tributaries in downstream locations are relatively much drier and adjust relatively slowly compared to

486   upstream locations. Interestingly, the trunk profile adjusts and communicates transient base-level signals

487   upstream to wetter tributaries relatively quickly compared to the adjustment timescale of these dry

488   tributaries, which follows as the trunk has much higher erosional efficiency from rainfall in its

489   headwaters. The initially counterintuitive result of this is that central portions of the catchment are the

490   first to achieve steady state (i.e., both the trunk profile and tributaries achieve the new steady state),

491   followed by the headwaters, and lastly tributaries near the outlet where the transient signal originated.

492   *4.3.3 Case 4: $k_{sn}–E_{avg}$ and $k_{sn-q}–E_{avg}$*

493   Evolution of $k_{sn}–E_{avg}$ and $k_{sn-q}–E_{avg}$ relationships during the transient evolution are generally similar to

494   Case 3, but a few aspects are notably different. First, the disparity between final steady state conditions

495   for the trunk profile and network of tributaries is significantly greater than Case 3 (Figures 6a, 6b), which

496   reflects the extent to which variations in erosional efficiency are buffered along the trunk profile by

497   concentrating rainfall near the headwaters. We also note that in $k_{sn-q}–E_{avg}$ space, apparent erosional

498   efficiency is more strongly affected during transient adjustment in the tributary network compared to the

499   trunk profile (transient deviations from the $K=K_p$ curve), but also compared to Case 3. Large deviations

500   are again restricted to drier tributary catchments, and comparison to Case 3 expresses that changes in

501   rainfall have a non-linear effect (Equations 1,7). That said, even these stronger effects on apparent

502   erosional efficiency in k_{sn-q}–E_{avg} space are still minor compared to representing any equivalent time in the

503   k_{sn}–E_{avg} relationship with a single erosional efficiency (K) value. Finally, also like Case 3, the range of

504   erosional efficiency values for the trunk profile ($K = \sim1.8 \cdot K_p$ to $2.25 \cdot K_p$) are different, in this case higher,

505   than is implied by mean rainfall (i.e., $K = \sim K_p$; Figures 1b, 6a) – discussed further in section 5.2.

5. Discussion

507   The central themes we have explored so far are how the spatial rainfall pattern influences the channel

508   profile morphology, and how temporal changes in rainfall pattern affect erosion rates and profile

509   morphology during periods of transient adjustment. We have detailed the expected response to along-

510   stream variations in erosional efficiency caused by spatial rainfall gradients according to the SPM and

511   have shown how the transient response to a change in rainfall pattern is fundamentally different from a

512   spatially uniform change in rainfall. A change in rainfall pattern will always result in spatio-temporally

513   variable changes in erosion rates, which in some circumstances means a given location may over time

514   experience both elevated and reduced erosion rates and channel steepness values relative to equilibrium in

515   response to a single change in rainfall. It is important to keep in mind, however, that the nature of

516   transient response depends strongly on the initial equilibrium conditions at the time of the change in

517   rainfall pattern. Therefore, there is a complex relationship between the transient response at any given

518   location or time and both the change in mean rainfall and the final rainfall pattern. In the following

519   discussion, we focus on highlighting some implications for the different expectations that follow from

520   changes in rainfall pattern. Specifically, we show some examples where conventional expectations based

521   on spatially uniform changes in rainfall can lead researchers astray, and where possible, we attempt to

522   identify additional information or strategies that may be leveraged by future studies to overcome these

523   challenges.

5.1 Revising Expectations for Erosional and Morphological Responses to Changing Climate
5.1.1 Relative Nature of Erosional Response

526   To this point, our choice of a steady state initial condition with spatially uniform rainfall has been

527   convenient, as have been the terms top-heavy and bottom-heavy to describe typical rainfall patterns.

528   While idealized, this provides an intuitive starting point for understanding how more complicated – but

529   almost certainly more realistic – climate change scenarios might play out. Recall, according to the SPM,

530   transient climate-driven changes in erosion rate are dictated by a *relative* change in discharge. Where

531   discharge is increased, erosion rates increase in response and river gradient declines toward a new

532   equilibrium steepness; thus, a river subjected to an increase in discharge can be considered locally, if

533   transiently, oversteepened relative to equilibrium, and vice versa. As we have shown, because discharge

534   generally accumulates non-linearly downstream within a river basin, a change in rainfall pattern can

535   readily create circumstances where the relative change in discharge inverts along the river length – at

536   position x_{sc} (Figure 2) – producing a complex transient response (Figures 2 & 3). Importantly, inversion

537   along the profile implies that the river is simultaneously oversteepened and understeepened on either side

538   of position x_{sc}, and these transient states dictate whether erosion rates initially increase or decrease

539   following the change in rainfall, respectively, not whether the new rainfall pattern is itself top-heavy or

540   bottom-heavy. The positions of these transient states then shift throughout adjustment.

541   The nature of landscape response to relative changes in discharge implies, for instance, that relaxation of

542   a bottom-heavy rainfall gradient can cause a complex transient response resembling a change from

543   uniform to top-heavy rainfall patterns. That is, a gentler bottom-heavy gradient is relatively top-heavy

544   compared to an extreme bottom-heavy gradient; similarly, a gentler top-heavy gradient is relatively

545   bottom-heavy compared to an extreme top-heavy gradient, and vice versa (Figure 7). Thus, for a change

546   in climate that causes an extreme bottom-heavy rainfall gradient to relax *and* results in a complex

547   transient response (e.g., Figure 7a), rainfall and erosion rate are expected to increase in the headwaters of

548   the catchment and decrease near the outlet. While the rainfall pattern is always bottom-heavy, this

549   expected erosional response is like the change from uniform to a top-heavy rainfall pattern described in

550   Case 4. This response, however, is not consistent with expectations for any uniform increase or decrease

551   in rainfall, even if such a shift accurately reflects the change in mean rainfall and rainfall pattern.

552   Therefore, neither the final rainfall pattern alone nor the relative change in mean rainfall (wetter or drier)

553   allow a robust prediction of changes in erosion rate within a catchment following a regional change in

554   climate.

555   Interestingly, changes in climate do not need to involve extreme changes in rainfall patterns (e.g., reversal

556   from top-heavy to bottom-heavy) to drive complex transient responses. Instead, a wide range of changes

557   to orographic patterns, including relatively subtle variations, that may reasonably be expected in response

558   to global climate changes, may significantly, if temporarily, alter the spatial pattern of erosion in a given

559   river basin. Because such complex, climate change-driven patterns of erosion are not reasonably captured

560   by a conceptual framework based on spatially uniform changes in rainfall, as documented above

561   (compare Cases 3 & 4 to Cases 1 & 2), apparent inconsistencies between expectations and observations

562   have the potential to give a false impression about the primary forcing(s) controlling erosion rates.

563   *5.1.2 Multi-stage Adjustment*

564   It has long been recognized that spatially uniform changes in rainfall should promote transient changes

565   erosion rate everywhere across a landscape, which causes morphological adjustments to sweep upstream

566   as erosional equilibrium is restored (e.g., Tucker & Slingerland, 1997; Whipple & Tucker, 1999). Our

567   model is fully consistent with this expectation under such conditions (e.g., Cases 1 & 2). In addition, we

568   have shown that responses to changes in the rainfall pattern are variable in both space and time (e.g.,

569   Cases 3 & 4). An important consequence of this is that following any non-uniform change in rainfall

570   pattern, distinct initial morphological and erosional changes always precede the upstream sweeping

571   adjustments that ultimately restore equilibrium. Thus, contrary to expectations for a uniform change in

572   rainfall, we find that catchments characteristically exhibit a relatively protracted, multi-stage, and spatio-

573   temporally variable response to a single change in rainfall pattern (Figure 8; Movie S5). We emphasize

574   that this behavior is a general characteristic of any non-uniform change in rainfall pattern and is not

575   exclusive to those that induce the complex transient responses. This leads to novel expectations for how

576   transient responses to changes in climate should be expressed across a landscape and has potentially

577   important implications for detecting transient landscape responses to climate changes.

578   The initial stage of morphological adjustment begins synchronously across the entire river basin

579   following a change in rainfall pattern. At the onset, local erosion rate is everywhere a function of the local

580   relative change in discharge for both trunk and tributary profiles, as described in Cases 3 & 4. As this

581   initial stage proceeds, spatial variations in erosion rate along the trunk river produce morphological

582   changes along its entire length that progress at different rates (variable erosional efficiency). Importantly,

583   this means that initial, or "relict", conditions are often not preserved upstream of slope-break knickpoints

584   on the trunk profile; the profile is progressively modified as adjustment proceeds even upstream of the

585   main knickpoint. Indeed, the resemblance of "unadjusted" profile segments upstream from the main

586   knickpoint to their initial state diminishes with time during the transient response, and thus with relative

587   position upstream. This contrasts with spatially uniform changes in rainfall (and erosional efficiency), or

588   uplift rate that does not affect erosional efficiency, that allow preservation of relict morphological

589   characteristics (e.g., k_{sn}) upstream of migrating transient knickpoints, as is often assumed in analysis and

590   inversions of river profiles (e.g., Clark et al., 2006; Fox et al., 2014; Gallen et al., 2013; Goren et al.,

591   2014; Kirby & Whipple, 2012; Miller et al., 2013; Schoenbohm et al., 2004; Whittaker et al., 2007). More

592   broadly, this contrasts with the notion that climate change should simply propagate upstream from base

593   level as is expected for other external changes (e.g., uplift rate). While there is a signal of transient

594   adjustment that indeed migrates upstream, significant amounts of surface uplift, as observed in Case 3

595   (Movie S3), or incision, as observed in Case 4 (Movie S4), along with changes in channel steepness can

596   occur prior to arrival of this signal. Nevertheless, these changes are in response to the change in climate.

597   Additionally, spatio-temporally variable adjustments along the trunk profile dictate that individual

598   tributaries experience temporally variable rates of base-level fall until the trunk profile reaches a new

599   equilibrium at their confluence (Movie S3 & S4).

600   The continuous, yet variable nature of base-level fall imposed by the trunk river on tributaries during the

601   initial stage of adjustment generally results in a broad adjustment zone characterized by smooth variations

602   in channel steepness in tributary catchments. Indeed, tributaries in our model located in upstream

603   positions where this initial adjustment stage is relatively long-lived (compared to tributaries located near

604   the trunk outlet) experience significant changes in slope and relief without formation of any knickpoints

605   (e.g., Figure 8b; Movies S3 & S4). Importantly, this shows that tributaries are not insulated from effects

606   of spatially variable changes in rainfall (variable erosional efficiency) along their trunk river, even if they

607   experience essentially uniform rainfall throughout their history. Furthermore, they may appear relatively

608   well-adjusted (graded) during periods of transient adjustment despite significant deviation from both

609   initial and final steady state conditions (Figure 8b; also see Tributary 2, Movies S3 & S4).

610   Adjustment to quasi-steady-state conditions along the trunk river, which may or may not be associated

611   with the upstream migration of a significant or obvious slope-break knickpoint, defines the beginning of

612   the second – and final – stage of adjustment in our model landscapes (Figure 8). The rate of base-level fall

613   experienced by a given tributary stabilizes upon local adjustment of the trunk profile, representing a

614   distinct change from the initial stage where the rate of base-level fall is temporally variable. Depending

615   on circumstances, this change may be abrupt and produce a discrete knickpoint that sweeps upstream

616   through the tributary catchment. The change in base-level fall rate is the dominant signal exhibited during

617   this second adjustment stage, although it acts upon the profile state reached during the initial adjustment

618   stage, and it is largely a function of the shape and migration rate of the trunk knickpoint. Both factors are

619   controlled by the integrated response of the trunk profile to this point, and therefore do not relate to the

620   change in rainfall pattern in a direct manner. Therefore, importantly, the dominant signal passed to

621   tributaries during this second stage, and any knickpoints that form as a result, generally do not reflect the

622   change in rainfall locally within the tributary catchment, and their relationship to the regional rainfall

623   pattern experienced by the trunk stream is complex. This is directly contrary to expectations for spatially

624   uniform changes in rainfall where changes in slope above and below knickpoints should scale with the

625   magnitude of the change in rainfall (e.g., Whipple, 2001).

626   Extrapolating these observations to natural, inherently more complex trellised river networks, suggests

627   that broad adjustment zones comprising multiple knickpoints might be associated with a given change in

628   rainfall pattern – in contrast to the single knickpoint or knickzone expected to accompany a spatially

629   uniform change in rainfall magnitude (e.g., Case 1 & 2). For instance, if second-order rivers (*sensu* Hack,

630   1957) experience spatially variable rainfall patterns in addition to the trunk, then we expect third-order

631   rivers should experience an additional pair of adjustment stages. Importantly, this analysis implies that the

632   full transient response to changes in rainfall pattern may be expressed in a complex fashion, and

633   potentially across a large areal extent, in large river basins (e.g., Figure 8; Movie S5). If true, this multi-

634   stage adjustment behavior may ultimately pose a significant, still unresolved, challenge to recognizing

635   and quantifying transient responses to changes in climate in many settings.

636   **5.2 The Influence of Climate on Topography and Erosion Rates**

637   *5.2.1 Steady State Relationships among Channel Steepness, Erosion Rate, and Erosional Efficiency*

638   The SPM makes specific predictions about the relationships among channel steepness, erosion rate, and

639   erosional efficiency (K) at steady state, as stated by Equations 7a & 7b and shown by curves in Figures 4-

640   6. Because the role of climate is encapsulated in K, it is important to remember that a uniform K value

641   implies that the influence of climate is uniform over the spatial and temporal scales of interest. Further,

642   the expectation that basin-average topographic metrics like k_{sn} should relate to rainfall in a simple way

643   generally relies on an assumption of a spatially uniform K value. Rainfall gradients systematically affect

644   this expectation, where bottom-heavy gradients result in higher k_{sn} (lower apparent erosional efficiency),

645   while top-heavy gradients result in lower k_{sn} (higher apparent erosional efficiency) (Figure 9). The

646   magnitude of this effect (as a percentage of actual erosional efficiency) varies with strength of the rainfall

647   gradient, but importantly, k_{sn} values also vary with uplift rate (Equation 7a). Therefore, while subtle

648   rainfall gradients affect apparent erosional efficiency to a proportionally lesser degree, they can still

649   substantially influence observed k_{sn} values where uplift rates are higher. This can be important in natural

650   settings where uplift rates, erosional efficiency, and the form of their relationship to topography are

651   generally unknown.

652   This analysis has two related, and important implications. First, interpretation of the controls on

653   topography (e.g., mean k_{sn}, mean gradient, relief, etc.) in terms of climate sensitivity, uplift, and/or rock

654   properties using measurements from catchments that experience the same mean rainfall, but different

655   rainfall patterns, is not necessarily valid even at steady state. Second, it predicts weaker correlations

656   (more dispersed) between topographic metrics and erosion rate than would be expected if rainfall were

657   always uniformly distributed, as is implied by use of basin-average rainfall (Figure 9). This prediction

658   applies even before considering any geologic uncertainties (e.g., at quasi-steady-state or potentially

659   transient?), analytical uncertainty, and even if no other variations in K exist. Because rainfall gradients

660   create systematic, rather than random, dispersion around relationships expected for uniformly distributed

661 rainfall, there is not necessarily any expectation that larger datasets will more accurately resolve

662 variations in erosional efficiency unless catchments where rainfall is uniform and are isolated, or a

663 correction is made for the influence of spatially variable rainfall (e.g., using k_{sn-q}). Rather, compilation of

664 topographic measurements from basins that do and do not experience rainfall gradients can, in and of

665 itself, obscure or, depending on circumstances, distort the actual influence of rainfall on erosional

666 efficiency (Figure 9). This result is of particular importance for designing future efforts to empirically test

667 the SPM in natural settings.

668 *5.2.2 Misleading Transient Signals*

669 Spatial patterns in erosion rate are commonly used to inform tectonic models and to infer rock uplift rates

670 in mountain landscapes (e.g., Adams et al., 2020; Godard et al., 2014; Kober et al., 2015; Morell et al.,

671 2015; Safran et al., 2005; Scherler et al., 2014). However, we have shown that changes in rainfall patterns

672 can drive long-lived and complex spatial patterns of erosion that differ from expectations for uniform

673 changes in rainfall (Whipple, 2001; Whipple & Tucker, 1999) and thus may not be readily recognized and

674 interpreted. We have also shown that that ongoing transient adjustment may not be obviously expressed

675 in landscape morphology (especially for catchment-mean metrics) under some circumstances. If these

676 caveats are not considered, subtly expressed transient spatial variations in erosion rate may be mistaken as

677 representing quasi-steady state spatial variations in uplift rate (i.e., $E = U$). At once this would give a false

678 impression about the spatial pattern of uplift and about the importance of past climate changes on

679 landscape evolution, with direct implications for understanding connections among climate, surface

680 processes, and tectonics. Determining whether there are circumstances in which spatial patterns of erosion

681 and topography produced by changes in rainfall patterns can be misleading enough to confound

682 interpretations is therefore critically important.

683 During the early transient adjustment in Case 3 (transition to a bottom-heavy rainfall pattern) there is a

684 clear example of circumstances where such confusion may occur (Figure 10). Recall, in this case, early

685 transient adjustment produces a concave-up knickpoint along the trunk profile but as it migrates upstream

686 the shape evolves. This creates a broad adjustment zone. Over the first ~500 kyr, quasi-steady state

687 adjustment proceeds ~60% upstream along the trunk, but the broad adjustment zone means most

688 tributaries along this length experience a protracted signal of base-level changes related to trunk

689 adjustment. Because these tributaries all also experience a net increase in rainfall, knickpoints associated

690 with local adjustment of the trunk river (Stage 2) tend to relax as they work upstream making them more

691 diffuse. This protracted competition between local rainfall and spatio-temporally variable rates of base-

692 level fall, generally results in diffuse concave to broad convexo-concave adjustment zones in tributaries

693   (e.g., Figure 8a; Movie S5). Broad adjustment zones, particularly concave-up adjustment zones, are

694   inherently subtle and this can inhibit their recognition. This problem may be further compounded by the

695   influence of sediment flux in natural settings (Brocard & Van Der Beek, 2006; Whipple & Tucker, 2002).

696   Indeed, even in our idealized model (i.e., no sediment influence), along-stream variations in trunk and

697   tributary local k_{sn} variation is diffuse (Figure 10c). Based on a lack of significant knickpoints that might

698   indicate transient adjustment and the several-fold spatial variation in erosion rate, one might reasonably

699   interpret relationships depicted in Figure 10a reflect a quasi-steady-state landscape adjusted to a spatial

700   gradient in uplift rate. In the absence of a surface breaking structures that might accommodate this

701   gradient in uplift, blind structures may be inferred, with potential implications for tectonic models. The

702   apparent viability of this interpretation is supported by the SPM if rock uplift rate is assumed to match the

703   observed pattern of catchment averaged erosion rates in tributaries (steady-state conditions) as illustrated

704   in Figure 10b. Figure 10b shows that the predicted steady-state upstream-averaged k_{sn} pattern along the

705   trunk river and mean k_{sn} values exhibited by the tributary network is essentially identical to the transient

706   pattern in Figure 10a. Moreover, even in detail, there are only subtle differences in the along-stream

707   pattern of local k_{sn} between the two scenarios (Figure 10c). Thus, in this instance, k_{sn} patterns and erosion

708   rates that actually record a complex transient response to a change in rainfall pattern could reasonably be

709   mistaken for a steady state landscape adjusted to a spatial gradient in uplift.

710   Importantly, we note that for this example the spatial pattern of $k_{sn\text{-}q}$ unambiguously suggests along-stream

711   variations in erosion rate exist along both the trunk river and tributaries. It also exhibits a coherent pattern

712   of downstream adjustment that could readily be interpreted as a transient signal sweeping upstream

713   through the catchment that, significantly, is inconsistent with a steady state landscape adjusted to the

714   spatial gradient in uplift shown in Figure 10b (Figure 10c). This example shows the potential usefulness

715   of $k_{sn\text{-}q}$, both as a diagnostic tool for detecting ongoing transient adjustment to changes in rainfall patterns

716   where k_{sn} may be misleading and for resolving the relative influences of tectonics and climate.

717   Finally, we emphasize that our intention is not to suggest all, or any specific examples, where spatial

718   patterns of rock uplift are inferred from erosion rates and channel steepness patterns are incorrect. Rather,

719   our intention here is to highlight the extent to which confusion may be possible under the right

720   circumstances, and how explicitly accounting for rainfall patterns can be a step toward addressing these

721   challenges.

722   **5.3 Toward Detecting the Influence of Climate on Topography and Erosion Rates**

723   As our various examples have shown, remote analysis of channel steepness patterns can provide a

724   preliminary means to detect whether spatial variations in rainfall may be influencing river profiles in a

725   landscape, and whether transient adjustment to a change in rainfall pattern may be ongoing. For

726   landscapes well-described by the SPM, discrepancies between rainfall conditions experienced by trunk

727   and tributary basins should cause systematic differences in trunk and tributary k_{sn} (Figures 5&6; Gasparini

728   & Whipple, 2014), but not in k_{sn-q}. As illustrated in Figure 10c, the expected contrast in trunk and

729   tributary k_{sn} is most developed at steady state, but it begins manifesting immediately during transient

730   adjustment as differences in local k_{sn} at confluences that migrate upstream (Figure 10c, Movie S5). In

731   contrast, precise agreement between trunk and tributary k_{sn-q} is expected at steady state, and it is

732   approximately maintained even during periods of adjustment to a change in rainfall pattern. In addition,

733   we note that agreement between trunk and tributary k_{sn-q} that weakens upstream from confluences may be

734   an important indication of ongoing transient adjustment that may be difficult detect from the k_{sn} pattern

735   alone (Figure 10c, e.g., as discussed in section 5.2.2). Therefore, comparison of k_{sn} and k_{sn-q} patterns may

736   at once be a potentially useful way to diagnose and further assess the potential extent of influence by

737   rainfall gradients, provided the pattern of discharge accumulation can be reasonably estimated (e.g., using

738   high spatial resolution satellite rainfall or nested stream gauge data).

739   Following topographic analysis, our results have additional implications for designing effective

740   catchment-averaged erosion rate sampling strategies. Broadly, sampling strategies can be grouped into

741   two classes: nested and distributed, described below. Nested, or hierarchical, sampling strategies comprise

742   multiple samples from the same river basin where some or all samples are collected along the trunk river,

743   and where averages typically integrate over very large (10^2–10^5 km^2) drainage areas (e.g., Abbühl et al.,

744   2010; Henck et al., 2011; Portenga et al., 2015; Reinhardt et al., 2007; Safran et al., 2005; Willenbring et

745   al., 2013). In principle, such strategies can allow researchers to assess reproducibility of individual

746   measurements, test sediment mixing models, and sub-divide basins into different sectors to identify

747   along-stream variations in erosion rates. Given the complex along-stream patterns of erosion rate we

748   observe in response to changing rainfall patterns and widely disparate responses between trunk and

749   tributary profiles, however, our results suggest that caution is warranted in interpreting patterns of erosion

750   rates collected in a nested fashion. In particular, this includes datasets that compile measurements from

751   along trunk rivers and tributary catchments, but also those that compare samples from different large

752   catchments that experience different mean climates and rainfall patterns, even at quasi-steady-state,

753   because how each reflects and experiences variations in rainfall may be fundamentally different.

754   Furthermore, because we find that along-stream variations in erosion rate due to changes in rainfall

755   pattern are characteristically muted along the trunk profile (e.g., Figure 10a), nested strategies may not be

756   appropriate in many settings, especially if the goal is to measure the influence of climate on fluvial

757   incision.

758   The other widely used strategy, which we refer to as a distributed sampling strategy, targets single
759   samples from catchments that are distributed across a landscape or mountain front, and typically – though
760   certainly not always – comprises relatively smaller (10^0-10^2 km^2) catchments (e.g., Adams et al., 2020;
761   Binnie et al., 2008; Carretier et al., 2013; DiBiase et al., 2010; Godard et al., 2014; Morell et al., 2015;
762   Ouimet et al., 2009; Scherler et al., 2014). This type of strategy generally allows more freedom to
763   carefully select preferable catchments (relatively uniform channel steepness, rainfall, lithology), with the
764   limitation that spatial variations in erosion at the sub-catchment scale are not resolvable with single
765   measurements. As a counter point to muted spatial variations in erosion noted for nested strategies, our
766   model results suggest this type of strategy inherently records a more direct signal of any climatic
767   influence. However, if inter-catchment variations in rainfall and therefore erosional efficiency are not
768   accounted for, or transient conditions are not recognized, this sensitivity may cause significant dispersion
769   or distortion in relationships among landscape metrics, as shown for k_{sn}–E_{avg} relationships (Figures 5b &
770   6b), and/or lead to misleading spatial patterns in erosion and channel steepness (Figure 10).

771   Lastly, we note that transient adjustments in response to changes in rainfall pattern do not significantly
772   affect apparent erosional efficiency in $k_{sn\text{-}q}$–E_{avg} relationships where no variations in rock properties exist,
773   even in response to the dramatic shifts in rainfall patterns that we model, regardless of sampling strategy.
774   Indeed, transient deviations from expected steady state relationships modelled in any location are
775   generally well within the analytical uncertainty of measured catchment-average erosion rates from natural
776   landscapes (Figures 5 and 6). Exceptions to this appear to be limited to scenarios where landscapes
777   experience a shift toward arid climates. Nevertheless, transient, spatially variable patterns of erosion due
778   to changes in rainfall pattern are reflected in $k_{sn\text{-}q}$ patterns with good accuracy in our model (Figure 10c,
779   Movie S3-S5), and thus $k_{sn\text{-}q}$ may be used to recognize ongoing adjustment to changes in climate where k_{sn}
780   can be ambiguous. Therefore, we suggest that $k_{sn\text{-}q}$, or a different metric that encompasses the spatial
781   distribution of rainfall (runoff), may be vital component for future efforts to detect climate's influence on
782   and from topography and erosion rates in mountain landscapes where rainfall is inherently spatially
783   variable.

784   **5.4 Caveats and Limitations**

785   Here we emphasize several important caveats should be kept in mind when evaluating the results and
786   subsequent discussion presented here. First, and foremost, our modelling efforts explicitly assume that
787   landscapes are inherently sensitive to climate (through rainfall) in a manner described by the SPM. While

788   the intuitive support for such sensitivity is strong, and evidence from natural landscapes is mounting that

789   broadly support predictions of the SPM (e.g., Adams, et al., 2020; Harel et al., 2016; Lague, 2014), there

790   remains a large amount of uncertainty about the strength of the sensitivity to climate.

791   Following the core assumption that the SPM is broadly applicable, we note that our model setup is very

792   simple. We assume that all precipitation is rainfall, all rainfall is converted directly to runoff, and we

793   impose constant rainfall gradients that act precisely along the trunk stream and basin axis and that span

794   the entire length of our modelled river basin. While some river basins set within mountain-belt scale

795   orographic precipitation patterns may indeed experience rainfall patterns consistent with this simple

796   geometry, we note that non-linear, and even non-monotonic, rainfall gradients are common for large river

797   basins or those characterized by high local relief (Roe, 2005). In addition, we model tributary catchments

798   that are uniform in size that experience uniform rainfall. Preliminary model investigations suggest that

799   although allowing tributary sizes and rainfall to vary causes some dispersion in the relationships

800   illustrated here, the overall behavior we describe remains the dominant signal. Nevertheless, both aspects

801   warrant further investigation.

802   Lastly, we emphasize that we use a simple version of the SPM where, among other simplifications, we

803   treat erosion exclusively as detachment limited. While assuming detachment-limited conditions is

804   common, particularly for describing erosion in mountain settings, it may not always be appropriate even

805   in these settings to describe transient behavior (Whipple & Tucker, 2002). Related to this, our treatment

806   of K_p, while incrementally more complex than spatially uniform erosional efficiency, remains highly

807   simplified. We do not explore the myriad of other factors that control erosional efficiency (K), and the

808   likelihood that rainfall, or more broadly climate, will influence rock erodibility ($\sim K_p$) and size distribution

809   of sediment delivered to rivers (Ferrier et al., 2013; Murphy et al., 2016; Neely & DiBiase, 2020; Riebe et

810   al., 2015; Sklar et al., 2017).

811   **6. Summary and Conclusions**

812   In this study, we use a simple form of the SPM to explore how spatial rainfall gradients influence both

813   river profiles and expectations about how fluvial landscapes should respond to changes in climate.

814   Notably, because changes in climate in mountain settings are likely to involve changes in precipitation

815   patterns, we expect that advancing understanding about how changes in climate influence the relief and

816   topographic form of mountain landscapes requires a more nuanced, spatially variable, treatment of

817   climate at the catchment scale beyond broadly characterized changes in mean climate. We show that

818   spatially varying rainfall conditions experienced by rivers occupying different landscape positions,

819 specifically trunk and tributary rivers, result in fundamentally different expressions of a given rainfall

820 pattern, and that they respond to changes in rainfall pattern in fundamentally different ways. Further, we

821 show how the non-linear nature discharge accumulation in a catchment means that even modest variations

822 in rainfall patterns can result in significant changes to spatial patterns of erosion and topography that

823 directly contrast with expectations for uniform changes in rainfall. In particular, changes in rainfall

824 pattern characteristically result in multi-stage responses with adjustment zones that can be both spatially

825 extensive and subtly expressed, thus difficult to recognize. Interestingly, these finding suggest more

826 broadly that catchments of different sizes, shapes, and locations set within regional orographic

827 precipitation patterns may have unique, and substantially variable, rainfall histories and responses to

828 changes in climate. These complications raise important questions about how best to interpret spatial

829 variations in erosion rates and their relation with topography, particularly from along-strike of orogenic

830 fronts where different transverse rivers may record broadly similar forcing in fundamentally different

831 ways. Finally, we show how catchment-scale variations in rainfall generally complicate relationships

832 between conventional topographic metrics (e.g., mean k_{sn}) and erosion rates, even at steady state, which

833 has implications for empirical tests of the SPM in natural landscapes. More precise metrics like k_{sn-q} that

834 leverage ever-increasing resolution of rainfall datasets to better account for the spatial distribution of

835 rainfall – specifically its effect on discharge and runoff – may be a significant step toward overcoming

836 these challenges, and may prove vital for future studies seeking to quantify interactions between climate,

837 tectonics, and erosion in mountain landscapes.

Acknowledgments

References

844 Abbühl, L. M., Norton, K. P., Schlunegger, F., Kracht, O., Aldahan, A., & Possnert, G. (2010). El Niño

845   forcing on 10Be-based surface denudation rates in the northwestern Peruvian Andes?

846   *Geomorphology*, *123*(3–4), 257–268. https://doi.org/10.1016/j.geomorph.2010.07.017

847 Adams, B. A., Whipple, K. X., Forte, A. M., Heimsath, A. M., & Hodges, K. V. (2020). Climate controls

848   on erosion in tectonically active landscapes. *Science Advances*, *6*(42), eaaz3166.

849   https://doi.org/10.1126/sciadv.aaz3166

850   Bierman, P., & Steig, E. J. (1996). Estimating Rates of Denudation Using Cosmogenic Isotope
851   Abundances in Sediment. *Earth Surface Processes and Landforms*, *21*(2), 125–139.
852   https://doi.org/10.1002/(sici)1096-9837(199602)21:2<125::aid-esp511>3.0.co;2-8

853   Binnie, S. A., Phillips, W. M., Summerfield, M. A., Fifield, L. K., & Spotila, J. A. (2008). Patterns of
854   denudation through time in the San Bernardino Mountains, California: Implications for early-stage
855   orogenesis. *Earth and Planetary Science Letters*, *276*(1–2), 62–72.
856   https://doi.org/10.1016/j.epsl.2008.09.008

857   Bonnet, S., & Crave, A. (2003). Landscape response to climate change: Insights from experimental
858   modeling and implications for tectonic versus climatic uplift of topography. *Geology*, *31*(2), 123–
859   126. https://doi.org/10.1130/0091-7613(2003)031<0123:LRTCCI>2.0.CO;2

860   Bookhagen, B., & Strecker, M. R. (2012). Spatiotemporal trends in erosion rates across a pronounced
861   rainfall gradient: Examples from the southern Central Andes. *Earth and Planetary Science Letters*,
862   *327–328*, 97–110. https://doi.org/10.1016/j.epsl.2012.02.005

863   Brocard, G. Y., & Van Der Beek, P. A. (2006). Influence of incision rate, rock strength, and bedload
864   supply on bedrock river gradients and valley-flat widths: Field-based evidence and calibrations from
865   western Alpine rivers (southeast France). *Special Paper of the Geological Society of America*, *398*,
866   101–126. https://doi.org/10.1130/2006.2398(07)

867   Brown, E. T., Stallard, R. F., Larsen, M. C., Raisbeck, G. M., & Yiou, F. (1995). Denudation rates
868   determined from the accumulation of in situ-produced 10Be in the luquillo experimental forest,
869   Puerto Rico. *Earth and Planetary Science Letters*, *129*(1–4), 193–202. https://doi.org/10.1016/0012-
870   821X(94)00249-X

871   Carretier, S., Regard, V., Vassallo, R., Aguilar, G., Martinod, J., Riquelme, R., et al. (2013). Slope and
872   climate variability control of erosion in the Andes of central Chile. *Geology*, *41*(2), 195–198.
873   https://doi.org/10.1130/G33735.1

874   Clark, M. K., Royden, L. H., Whipple, K. X., Burchfiel, B. C., Zhang, X., & Tang, W. (2006). Use of a
875   regional, relict landscape to measure vertical deformation of the eastern Tibetan Plateau. *Journal of
876   Geophysical Research: Earth Surface*, *111*(3), 1–23. https://doi.org/10.1029/2005JF000294

877   Cyr, A. J., Granger, D. E., Olivetti, V., & Molin, P. (2014). Distinguishing between tectonic and
878   lithologic controls on bedrock channel longitudinal profiles using cosmogenic 10Be erosion rates
879   and channel steepness index. *Geomorphology*, *209*, 27–38.
880   https://doi.org/10.1016/j.geomorph.2013.12.010

881   D'Arcy, M., & Whittaker, A. C. (2014). Geomorphic constraints on landscape sensitivity to climate in
882   tectonically active areas. *Geomorphology*, *204*, 366–381.
883   https://doi.org/10.1016/j.geomorph.2013.08.019

884   Darling, A., Whipple, K., Bierman, P., Clarke, B., & Heimsath, A. (2020). Resistant rock layers amplify
885   cosmogenically-determined erosion rates. *Earth Surface Processes and Landforms*, *45*(2), 312–330.
886   https://doi.org/10.1002/esp.4730

887   DiBiase, R. A., Whipple, K. X., Heimsath, A. M., & Ouimet, W. B. (2010). Landscape form and
888   millennial erosion rates in the San Gabriel Mountains, CA. *Earth and Planetary Science Letters*,
889   *289*(1–2), 134–144. https://doi.org/10.1016/j.epsl.2009.10.036

890   Duvall, A. (2004). Tectonic and lithologic controls on bedrock channel profiles and processes in coastal
891   California. *Journal of Geophysical Research*, *109*(F3), 1–18. https://doi.org/10.1029/2003jf000086

892   Ferrier, K. L., Huppert, K. L., & Perron, J. T. (2013). Climatic control of bedrock river incision. *Nature*,
893   *496*(7444), 206–209. https://doi.org/10.1038/nature11982

894   Forte, A. M., Yanites, B. J., & Whipple, K. X. (2016). Complexities of landscape evolution during
895   incision through layered stratigraphy with contrasts in rock strength. *Earth Surface Processes and
896   Landforms*, *41*(12), 1736–1757. https://doi.org/10.1002/esp.3947

897   Fox, M., Goren, L., May, D. A., & Willett, S. D. (2014). Inversion of fluvial channels for paleorock uplift
898   rates in Taiwan. *Journal of Geophysical Research: Earth Surface*, *119*(9), 1853–1875.
899   https://doi.org/10.1002/2014jf003196

900   Gallen, S. F., Wegmann, K. W., & Bohnenstiehl, D. W. R. (2013). Miocene rejuvenation of topographic
901   relief in the southern Appalachians. *GSA Today*, *23*(2), 4–10.
902   https://doi.org/10.1130/GSATG163A.1

903   Gasparini, N. M., & Whipple, K. X. (2014). Diagnosing climatic and tectonic controls on topography:
904   Eastern flank of the northern Bolivian Andes. *Lithosphere*, *6*(4), 230–250.
905   https://doi.org/10.1130/L322.1

906   Gasparini, N. M., Bras, R. L., & Whipple, K. X. (2006). Numerical modeling of non–steady-state river
907   profile evolution using a sediment-flux-dependent incision model. In S. D. Willett, N. Hovius, M. T.
908   Brandon, & D. M. Fisher (Eds.), *Tectonics, Climate, and Landscape Evolution* (Vol. 398, p. 0).
909   Geological Society of America. https://doi.org/10.1130/2006.2398(08)

910   Gasparini, N. M., Whipple, K. X., & Bras, R. L. (2007). Predictions of steady state and transient
911   landscape morphology using sediment-flux-dependent river incision models. *Journal of Geophysical*

912   *Research: Earth Surface*, *112*(3), 1–20. https://doi.org/10.1029/2006JF000567

913   Godard, V., Bourlès, D. L., Spinabella, F., Burbank, D. W., Bookhagen, B., Fisher, G. B., et al. (2014).

914   Dominance of tectonics over climate in himalayan denudation. *Geology*, *42*(3), 243–246.

915   https://doi.org/10.1130/G35342.1

916   Goren, L., Fox, M., & Willett, S. D. (2014). Tectonics from fluvial topography using formal linear

917   inversion: Theory and applications to the Inyo Mountains, California. *Journal of Geophysical*

918   *Research F: Earth Surface*, *119*(8), 1651–1681. https://doi.org/10.1002/2014JF003079

919   Granger, D. E., Kirchner, J. W., & Finkel, R. (1996). Spatially averaged long-term erosion rates measured

920   from in situ-produced cosmogenic nuclides in alluvial sediment. *Journal of Geology*, *104*(3), 249–

921   257. https://doi.org/10.1086/629823

922   Hack, J. T. (1957). *Studies of Longitudinal Stream Profiles in Virginia and Maryland*. Retrieved from

923   https://pubs.usgs.gov/pp/0294b/report.pdf

924   Han, J., Gasparini, N. M., Johnson, J. P. L., & Murphy, B. P. (2014). Modeling the influence of rainfall

925   gradients on discharge, bedrock erodibility, and river profile evolution, with application to the Big

926   Island, Hawai'i. *Journal of Geophysical Research: Earth Surface*, *119*(6), 1418–1440.

927   https://doi.org/10.1002/2013JF002961

928   Han, J., Gasparini, N. M., & Johnson, J. P. L. (2015). Measuring the imprint of orographic rainfall

929   gradients on the morphology of steady-state numerical fluvial landscapes. *Earth Surface Processes*

930   *and Landforms*, *40*(10), 1334–1350. https://doi.org/10.1002/esp.3723

931   Harel, M. A., Mudd, S. M., & Attal, M. (2016). Global analysis of the stream power law parameters based

932   on worldwide 10Be denudation rates. *Geomorphology*, *268*, 184–196.

933   https://doi.org/10.1016/j.geomorph.2016.05.035

934   Henck, A. C., Huntington, K. W., Stone, J. O., Montgomery, D. R., & Hallet, B. (2011). Spatial controls

935   on erosion in the Three Rivers Region, southeastern Tibet and southwestern China. *Earth and*

936   *Planetary Science Letters*, *303*(1–2), 71–83. https://doi.org/10.1016/j.epsl.2010.12.038

937   Howard, A. D. (1994). A detachment-limited model of drainage basin evolution. *Water Resources*

938   *Research*, *30*(7), 2261–2285. https://doi.org/10.1029/94WR00757

939   Howard, A. D., & Kerby, G. (1983). Channel changes in badlands. *Geological Society of America*

940   *Bulletin*, *94*, 739–752.

941   Insel, N., Ehlers, T. A., Schaller, M., Barnes, J. B., Tawackoli, S., & Poulsen, C. J. (2010). Spatial and

942   temporal variability in denudation across the Bolivian Andes from multiple geochronometers.

943   *Geomorphology*, *122*(1–2), 65–77. https://doi.org/10.1016/j.geomorph.2010.05.014

944 Kirby, E., & Whipple, K. X. (2012). Expression of active tectonics in erosional landscapes. *Journal of*
945   *Structural Geology*, *44*, 54–75. https://doi.org/10.1016/j.jsg.2012.07.009

946 Kober, F., Zeilinger, G., Hippe, K., Marc, O., Lendzioch, T., Grischott, R., et al. (2015). Tectonic and
947   lithological controls on denudation rates in the central Bolivian Andes. *Tectonophysics*, *657*, 230–
948   244. https://doi.org/10.1016/j.tecto.2015.06.037

949 Lague, D. (2014). The stream power river incision model: Evidence, theory and beyond. *Earth Surface*
950   *Processes and Landforms*, *39*(1), 38–61. https://doi.org/10.1002/esp.3462

951 Miller, S. R., Sak, P. B., Kirby, E., & Bierman, P. R. (2013). Neogene rejuvenation of central
952   Appalachian topography: Evidence for differential rock uplift from stream profiles and erosion rates.
953   *Earth and Planetary Science Letters*, *369–370*(May), 1–12.
954   https://doi.org/10.1016/j.epsl.2013.04.007

955 Molnar, P. (2001). Climate change, flooding in arid environments, and erosion rates. *Geology*, *29*(12),
956   1071–1074. https://doi.org/10.1130/0091-7613(2001)029<1071:CCFIAE>2.0.CO

957 Morell, K. D., Sandiford, M., Rajendran, C. P., Rajendran, K., Alimanovic, A., Fink, D., & Sanwal, J.
958   (2015). Geomorphology reveals active décollement geometry in the central Himalayan seismic gap.
959   *Lithosphere*, *7*(3), 247–256. https://doi.org/10.1130/L407.1

960 Murphy, B. P., Johnson, J. P. L., Gasparini, N. M., & Sklar, L. S. (2016). Chemical weathering as a
961   mechanism for the climatic control of bedrock river incision. *Nature*, *532*(7598), 223–227.
962   https://doi.org/10.1038/nature17449

963 Neely, A. B., & DiBiase, R. A. (2020). Drainage area, bedrock fracture spacing, and weathering controls
964   on landscape-scale patterns in surface sediment grain size. *Earth and Space Science Open Archive*,
965   1–22. https://doi.org/10.1002/essoar.10502617.1

966 Olen, S. M., Bookhagen, B., & Strecker, M. R. (2016). Role of climate and vegetation density in
967   modulating denudation rates in the Himalaya. *Earth and Planetary Science Letters*, *445*, 57–67.
968   https://doi.org/10.1016/j.epsl.2016.03.047

969 Ouimet, W. B., Whipple, K. X., & Granger, D. E. (2009). Beyond threshold hillslopes: Channel
970   adjustment to base-level fall in tectonically active mountain ranges. *Geology*, *37*(7), 579–582.
971   https://doi.org/10.1130/G30013A.1

972 Perron, J. T. (2017). Climate and the Pace of Erosional Landscape Evolution. *Annual Review of Earth and*
973   *Planetary Sciences*, *45*(1), 561–591. https://doi.org/10.1146/annurev-earth-060614-105405

974   Portenga, E. W., Bierman, P. R., Duncan, C., Corbett, L. B., Kehrwald, N. M., & Rood, D. H. (2015).
975   Erosion rates of the Bhutanese Himalaya determined using in situ-produced 10Be. *Geomorphology*,
976   *233*, 112–126. https://doi.org/10.1016/j.geomorph.2014.09.027

977   Reinhardt, L. J., Bishop, P., Hoey, T. B., Dempster, T. J., & Sanderson, D. C. W. (2007). Quantification
978   of the transient response to base-level fall in a small mountain catchment: Sierra Nevada, southern
979   Spain. *Journal of Geophysical Research: Earth Surface*, *112*(3).
980   https://doi.org/10.1029/2006JF000524

981   Riebe, C. S., Sklar, L. S., Lukens, C. E., & Shuster, D. L. (2015). Climate and topography control the size
982   and flux of sediment produced on steep mountain slopes. *Proceedings of the National Academy of
983   Sciences of the United States of America*, *112*(51), 15574–15579.
984   https://doi.org/10.1073/pnas.1503567112

985   Rigon, R., Rodriguez-Iturbe, I., Maritan, A., Giacometti, A., Tarboton, D. G., & Rinaldo, A. (1996). On
986   Hack's Law. *Water Resources Research*, *32*(11), 3367–3374. https://doi.org/10.1029/96WR02397

987   Riihimaki, C. A., Anderson, R. S., & Safran, E. B. (2007). Impact of rock uplift on rates of late Cenozoic
988   Rocky Mountain river incision. *Journal of Geophysical Research: Earth Surface*, *112*(3), 1–15.
989   https://doi.org/10.1029/2006JF000557

990   Rinaldo, A., Dietrich, W. E., Rigon, R., Vogel, G. K., & Rodrlguezlturbe, I. (1995). Geomorphological
991   signatures of varying climate. *Nature*, *374*(6523), 632–635. https://doi.org/10.1038/374632a0

992   Roe, G. H. (2005). Orographic Precipitation. *Annual Review of Earth and Planetary Sciences*, *33*(1), 645–
993   671. https://doi.org/10.1146/annurev.earth.33.092203.122541

994   Roe, G. H., Montgomery, D. R., & Hallet, B. (2002). Effects of orographic precipitation variations on the
995   concavity of steady-state river profiles. *Geology*, *30*(2), 143–146. https://doi.org/10.1130/0091-
996   7613(2002)030<0143:EOOPVO>2.0.CO;2

997   Roe, G. H., Montgomery, D. R., & Hallet, B. (2003). Orographic precipitation and the relief of mountain
998   ranges. *Journal of Geophysical Research: Solid Earth*, *108*(B6).
999   https://doi.org/10.1029/2001jb001521

1000 Roe, G. H., Whipple, K. X., & Fletcher, J. K. (2008). Feedbacks among climate, erosion, and tectonics in
1001   a critical wedge orogen. *American Journal of Science*, *308*(7), 815–842.
1002   https://doi.org/10.2475/07.2008.01

1003 Royden, L., & Perron, J. T. (2013). Solutions of the stream power equation and application to the
1004   evolution of river longitudinal profiles. *Journal of Geophysical Research: Earth Surface*, *118*(2),

1005   497–518. https://doi.org/10.1002/jgrf.20031

1006 Safran, E. B., Bierman, P. R., Aalto, R., Dunne, T., Whipple, K. X., & Caffee, M. (2005). Erosion rates

1007   driven by channel network incision in the Bolivian Andes. *Earth Surface Processes and Landforms*,

1008   *30*(8), 1007–1024. https://doi.org/10.1002/esp.1259

1009 Scherler, D., Bookhagen, B., & Strecker, M. R. (2014). Tectonic control on 10Be-derived erosion rates in

1010   the Garhwal Himalaya, India. *Journal of Geophysical Research: Earth Surface*, *119*(2), 83–105.

1011   https://doi.org/10.1002/2013JF002955

1012 Scherler, D., DiBiase, R. A., Fisher, G. B., & Avouac, J. P. (2017). Testing monsoonal controls on

1013   bedrock river incision in the Himalaya and Eastern Tibet with a stochastic-threshold stream power

1014   model. *Journal of Geophysical Research: Earth Surface*, *122*(7), 1389–1429.

1015   https://doi.org/10.1002/2016JF004011

1016 Schoenbohm, L. M., Whipple, K. X., Burchfiel, B. C., & Chen, L. (2004). Geomorphic constraints on

1017   surface uplift, exhumation, and plateau growth in the Red River region, Yunnan Province, China.

1018   *Bulletin of the Geological Society of America*, *116*(7–8), 895–909. https://doi.org/10.1130/B25364.1

1019 Sklar, L. S., Riebe, C. S., Marshall, J. A., Genetti, J., Leclere, S., Lukens, C. L., & Merces, V. (2017). The

1020   problem of predicting the size distribution of sediment supplied by hillslopes to rivers.

1021   *Geomorphology*, *277*, 31–49. https://doi.org/10.1016/j.geomorph.2016.05.005

1022 Tucker, G E, & Whipple, K. X. (2002). Topographic outcomes predicted by stream erosion models:

1023   Sensitivity analysis and intermodel comparison. *Journal of Geophysical Research: Solid Earth*,

1024   *107*(B9), ETG 1-1-ETG 1-16. https://doi.org/10.1029/2001jb000162

1025 Tucker, Gregory E., & Slingerland, R. (1997). Drainage basin responses to climate change. *Water*

1026   *Resources Research*, *33*(8), 2031–2047. https://doi.org/10.1029/97WR00409

1027 Vanacker, V., von Blanckenburg, F., Govers, G., Molina, A., Campforts, B., & Kubik, P. W. (2015).

1028   Transient river response, captured by channel steepness and its concavity. *Geomorphology*, *228*,

1029   234–243. https://doi.org/10.1016/j.geomorph.2014.09.013

1030 Ward, D. J., & Galewsky, J. (2014). Exploring landscape sensitivity to the Pacific Trade Wind Inversion

1031   on the subsiding island of Hawaii. *Journal of Geophysical Research: Earth Surface*, *119*(9), 2048–

1032   2069. https://doi.org/10.1002/2014JF003155

1033 Whipple, K. X. (2001). Fluvial landscape response time: How plausible is steady-state denudation?

1034   *American Journal of Science*, *301*(4–5), 313–325. https://doi.org/10.2475/ajs.301.4-5.313

1035 Whipple, K. X., & Meade, B. J. (2006). Orogen response to changes in climatic and tectonic forcing.

1036   *Earth and Planetary Science Letters*, *243*(1–2), 218–228. https://doi.org/10.1016/j.epsl.2005.12.022

1037 Whipple, K. X., & Tucker, G. E. (1999). Dynamics of the stream-power river incision model:

1038   Implications for height limits of mountain ranges, landscape response timescales, and research

1039   needs. *Journal of Geophysical Research: Solid Earth*, *104*(B8), 17661–17674.

1040   https://doi.org/10.1029/1999jb900120

1041 Whipple, K. X., & Tucker, G. E. (2002). Implications of sediment-flux-dependent river incision models

1042   for landscape evolution. *Journal of Geophysical Research*, *107*(B2), 2039.

1043   https://doi.org/10.1029/2000jb000044

1044 Whittaker, A. C. (2012). How do landscapes record tectonics and climate? *Lithosphere*, *4*(2), 160–164.

1045   https://doi.org/10.1130/RF.L003.1

1046 Whittaker, A. C., Cowie, P. A., Attal, M., Tucker, G. E., & Roberts, G. P. (2007). Bedrock channel

1047   adjustment to tectonic forcing: Implications for predicting river incision rates. *Geology*, *35*(2), 103–

1048   106. https://doi.org/10.1130/G23106A.1

1049 Willenbring, J. K., Gasparini, N. M., Crosby, B. T., & Brocard, G. (2013). What does a mean mean? The

1050   temporal evolution of detrital cosmogenic denudation rates in a transient landscape. *Geology*,

1051   *41*(12), 1215–1218. https://doi.org/10.1130/G34746.1

1052 Wittmann, H., Malusà, M. G., Resentini, A., Garzanti, E., & Niedermann, S. (2016). The cosmogenic

1053   record of mountain erosion transmitted across a foreland basin: Source-to-sink analysis of in situ

1054   10Be, 26Al and 21Ne in sediment of the Po river catchment. *Earth and Planetary Science Letters*,

1055   *452*, 258–271. https://doi.org/10.1016/j.epsl.2016.07.017

1056 Wobus, C., Whipple, K. X., Kirby, E., Snyder, N., Johnson, J., Spyropolou, K., et al. (2006). Tectonics

1057   from topography: Procedures, promise, and pitfalls. *Special Paper of the Geological Society of*

1058   *America*, *398*(04), 55–74. https://doi.org/10.1130/2006.2398(04)

1059

1060 **Figures and Tables**

Table 1. Model Parameters

Parameters	Value	Units
U	5.0 x 10^{-4}	m·yr^{-1}
K_p	2.5 x 10^{-9}	m^{-1}·yr^{-1}
m	1	
n	2	

k_a	6.69	
h	1.67	
L		
Trunk	50	km
Tributaries	5	km
A		
Trunk	472	km²
Tributaries	11	km²
A_c	1	km²
Node spacing	25	m
Time step	50	yr
Tributary Spacing	1	km

1061
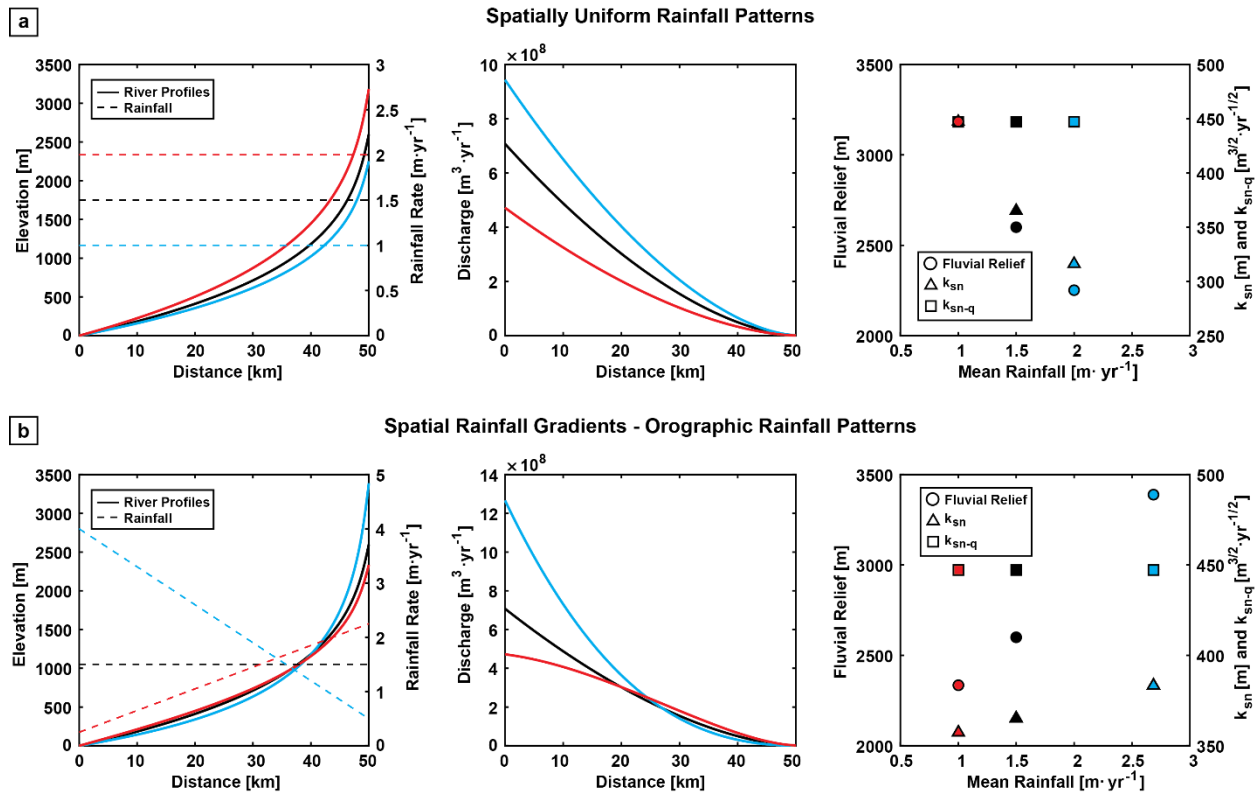
1062

1063   **Figure 1**. Influence of rainfall on channel profile form and topographic metrics at steady state. a) Top row
1064   – left panel shows river profiles adjusted to spatially uniform 1, 1.5, and 2 m/yr of rainfall (dashed, solid,
1065   and dotted, respectively). Corresponding discharge accumulation curves are shown in the middle panel.
1066   Right panel shows the relationship between mean rainfall (defined as Q/A) calculated at the outlet, with
1067   fluvial relief (R), k_{sn}, and k_{sn-q} for a fixed uniform rock uplift rate. Note, at steady state fluvial relief and k_{sn}
1068   are inversely related to mean rainfall, while k_{sn-q} is independent of changes in rainfall. b) Bottom row – all
1069   panels as in (a) but for a comparable suite of steady-state profiles adjusted to uniform 1.5 m/yr of rainfall,
1070   rainfall decreasing upstream from 4 to 0.5 m/yr, and rainfall increasing upstream from 0.25 to 2.25 m/yr.

36

1071   Note intersections that occur between profiles in the left panel, and in downstream discharge (middle
1072   panel), and that fluvial relief and k_{sn} are positively related to mean rainfall in these cases (right panel),
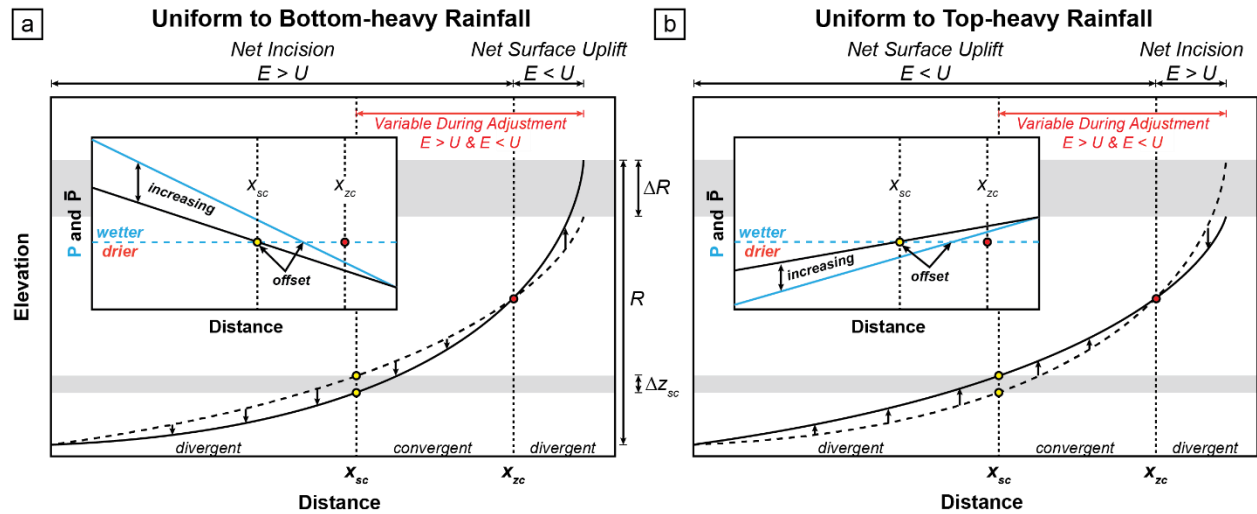1073   inverted from (a). All other model parameters are equal (see Table 1).

1074

1075   **Figure 2**. Schematic illustration of key aspects of complex transient river profile responses – defined in
1076   section 3.3 – that can result due to changes from spatially uniform rainfall (initial) to a bottom-heavy (a)
1077   and top-heavy rainfall gradient (b) – rainfall shown in inset. Initial and final steady state river profiles
1078   shown in dashed and solid black lines, respectively. Horizontal grey bars highlight net change in fluvial
1079   relief (ΔR) and the maximum amount of enhanced incision (Δz_{sc}) along the profile due to change in
1080   rainfall. Colored circles mark positions of x_{sc} (yellow) and x_{zc} (red) – see text for definition and discussion
1081   of these points – that also demarcate segments of net divergent and convergent transient adjustments.
1082   Domains of net mode of transient adjustment indicated along top axis. Note reversal at position x_{zc} (net
1083   incision downstream, net uplift upstream); however, during transience, adjustment upstream of x_{sc} is
1084   variable with time. Inset shows both initial local rainfall rate (P) and upstream averaged rainfall ($\overline{P}$) in
1085   blue dashed line; $P = \overline{P}$ for spatially uniform rainfall. Solid lines show final local rainfall rate (blue) and
1086   final upstream averaged rainfall (black). Positions of x_{sc} and x_{zc} in inset correspond to those along the
1087   profiles in the main figure. Note along-stream offset in position where P and $\overline{P}$ exceed the initial rainfall
1088   rate, the latter corresponding to x_{sc}. Also, note that the difference between P and $\overline{P}$ increases
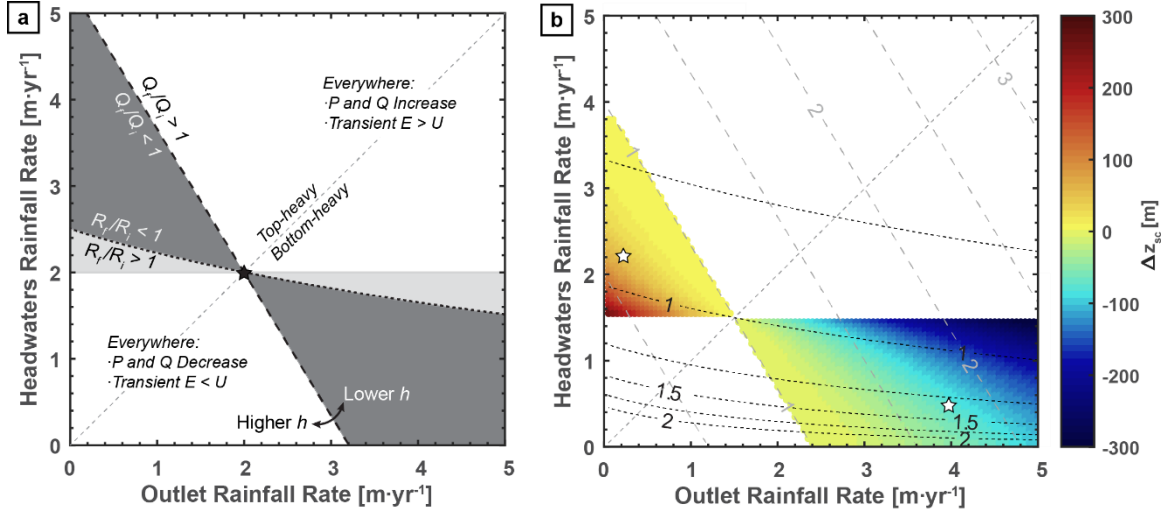1089   systematically downstream.

1090

Figure 3. Sensitivity analysis of a river profile to different spatial gradients in rainfall. a) Defines general domains of behavior described in the sensitivity analysis shown in (b) – see text for descriptions of different fields. Black star in (a) marks the initial condition; note, initial conditions in panels (a) and (b) are different. Top-heavy and bottom-heavy domains are separated by the 1:1 line. The primary influence of different h values in Hack's relationship is on the slope of Q_f/Q_i, as indicated. b) Same as (a) but where the initial profile is adjusted to spatially uniform $P = 1.5$ m/yr, as in Figure 1, and grey fields in (a) are colored by magnitude of Δz_{sc} (e.g., Figure 2; see text for more discussion). White stars show rainfall gradient scenarios explored in section 3 – Cases 3 & 4. Contours of Q_f/Q_i are shown in grey dashed lines, and contours of R_f/R_i in black dotted lines.
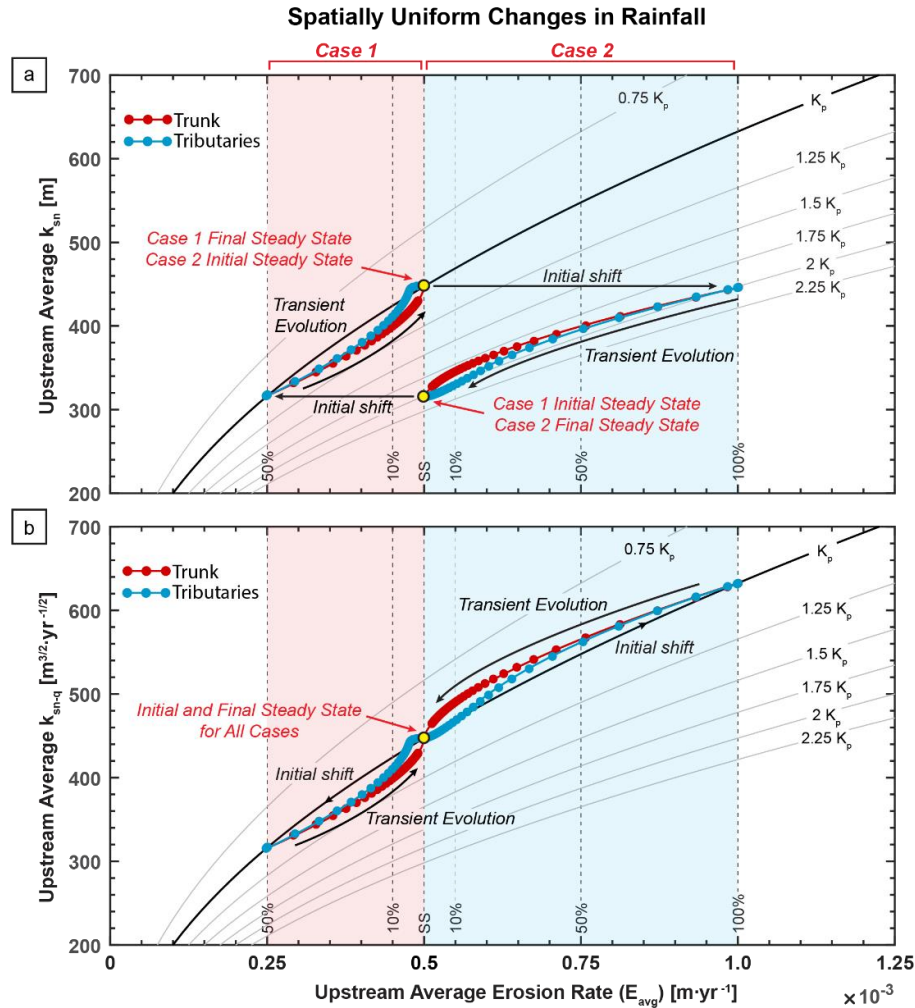
Figure 4. Representative time slice of transient evolution for Case 1 (uniform decrease in rainfall from 2 m/yr to 1 m/yr) and Case 2 (uniform increase in rainfall from 1 m/yr to 2 m/yr) through (a) k_{sn}-E_{avg} and (b) k_{sn-q}-E_{avg} parameter spaces. Case 1 is shown in red shaded domain (transient decrease in erosion rate, $E < U$), and Case 2 is in blue shaded domain (transient increase in erosion rate, $E > U$). Curves expressing the expected steady state relationship between channel steepness and erosion rate with different uniform erosional efficiencies are shown; $K = K_p$, shown in black solid line, and grey lines show different values of K as multiples of K_p. Vertical dashed lines show percent deviations from steady state erosion rate. Initial and final conditions shown with yellow circles, as labelled. Model data from different positions along the trunk profile and individual tributaries shown with red and blue data points, respectively. Trunk data shown are only profile nodes at tributary junctions – all trunk profile datapoints have a corresponding tributary datapoint at the same position within the modelled landscape. Trunk profile data show upstream mean values from their respective position, and tributary data show mean values for the entire tributary profile (i.e., at the junction with the trunk profile).
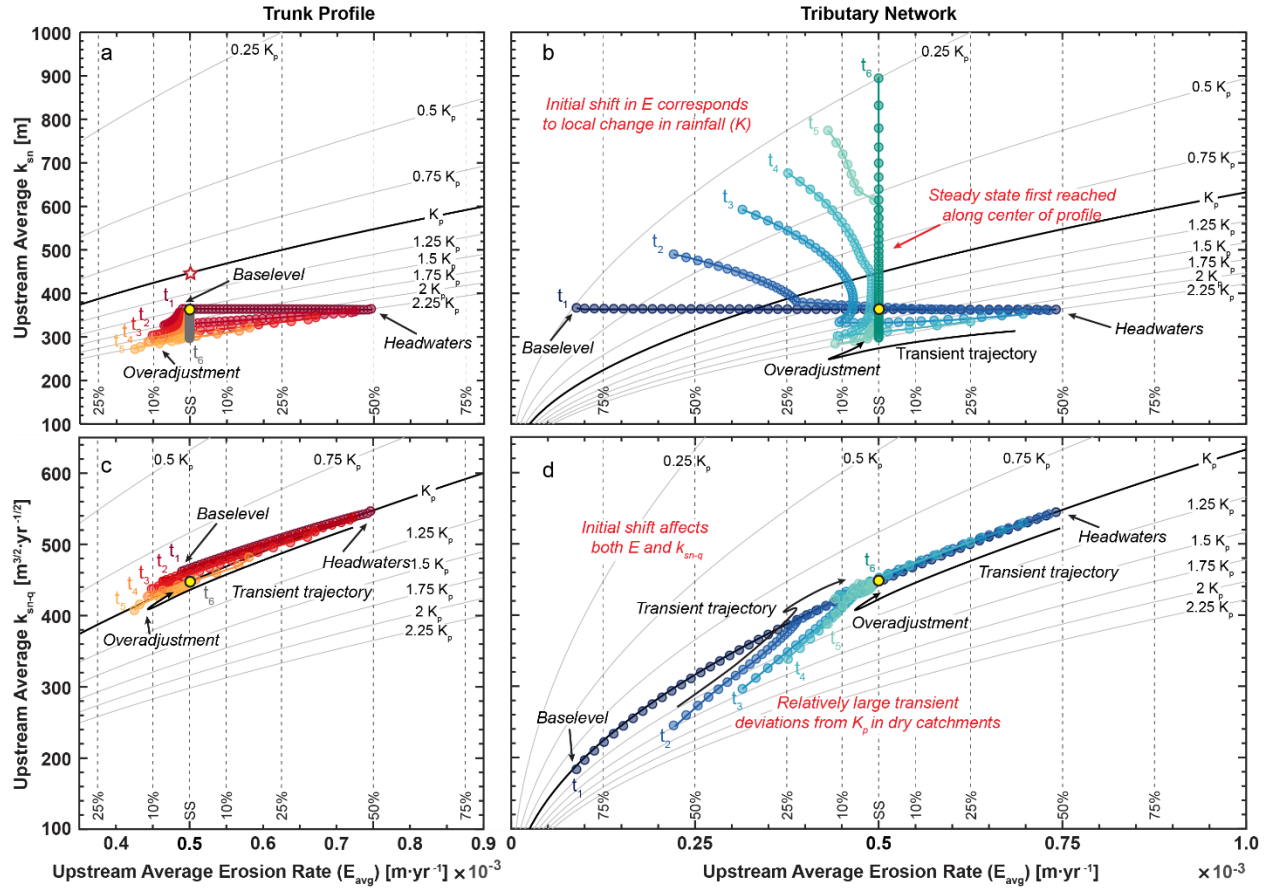
Figure 5. Transient evolution of the trunk profile (a & c) and network of tributaries (b & d) in Case 3 (spatially uniform $P = 1.5$ m/yr to gradient decreasing upstream from 4 to 0.5 m/yr) through k_{sn}-E_{avg} (a & b) and k_{sn-q}-E_{avg} (b & d) parameter spaces. Layout of individual panels is like Figure 4. Six representative time slices are shown; t_1 shows time at 10 kyr model time (i.e., first time step at following change in rainfall), t_6 is at final steady state. Time intervals are not evenly spaced, but t_1-t_6 are the same time-step for all panels. Note range in k_{sn} values, and related erosional efficiency values, spanned at final steady state in panels (a) and (b). Also, the range of responses by trunk profile during transient adjustment is significantly reduced relative to the network of tributaries in both k_{sn} and k_{sn-q}. Star in panel (a) shows expected erosional efficiency calculated from equation (1b) based on the final mean rainfall of 2.68 m/yr ($2.68 \cdot K_p$) at steady state, which corresponds to a predicted mean k_{sn} of ~275. Note offset between this value and range of erosional efficiency and k_{sn} values spanned by trunk profile.

Figure 6. Transient evolution of the trunk profile (a & c) and network of tributaries (b & d) in Case 4 (spatially uniform P = 1.5 m/yr to gradient increasing upstream from 0.25 to 2.25 m/yr) through k_{sn}-E_{avg} (a & b) and k_{sn-q}-E_{avg} (c & d) parameter spaces; figure layout is same as Figure 5. Like Case 3, the range in k_{sn} and k_{sn-q} values in trunk stream response is significantly less than in the network of tributaries. However, note relatively larger disparity between the range k_{sn} and erosional efficiency (K) spanned by the trunk profile and the network of tributaries at final steady state (a & b). Transient deviations from curve for K_p in panel (d) are also relatively larger than in Case 3, which is consistent with the fact that these tributaries are much drier – discussed further in section 5.1. Star in panel (a) shows K calculated from equation (1b) based on the final mean rainfall of 1 m/yr ($K = K_p$) at steady state, which corresponds to a predicted mean k_{sn} of ~450. Again, note offset between this value and range of erosional efficiency and k_{sn} values spanned by trunk profile.
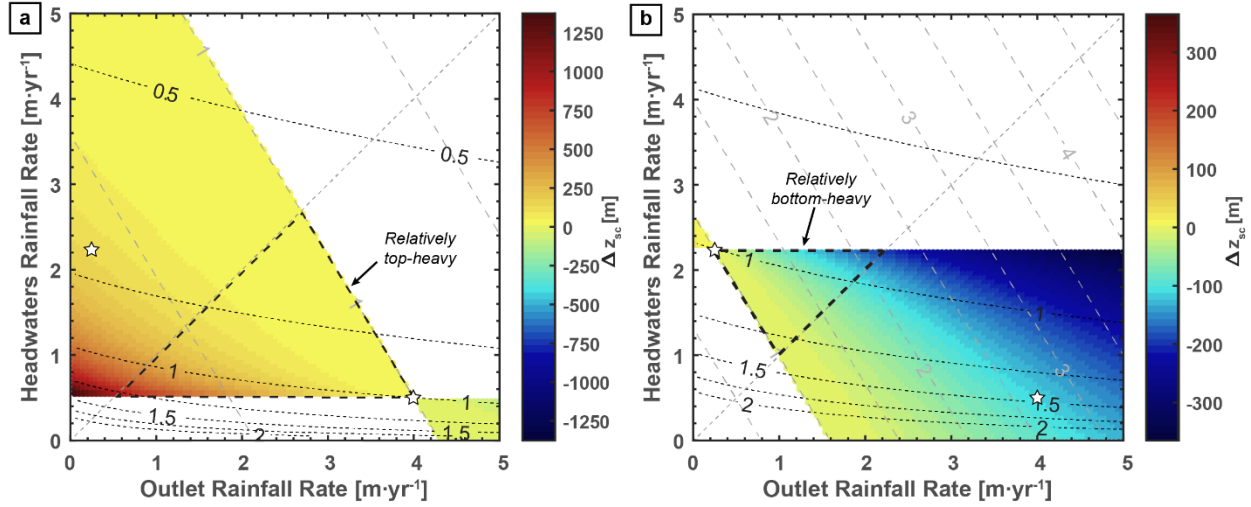
Figure 7. Sensitivity analysis where initial conditions are rainfall patterns used in Case 3 (a) bottom heavy – decreasing upstream from 4 to 0.5 m/yr – and top heavy gradient from Case 4 (b) – increasing upstream from 0.25 to 2.25 m/yr. Panel layouts are the same as in Figure 3b. Triangular fields demarcated in black dashes bound rainfall gradients with the same pattern as the initial condition (i.e., bottom-heavy or top-heavy), but cause complex transient responses similar to those expected for reversals in polarity of the rainfall pattern as the rainfall becomes *relatively* more or less bottom- or top-heavy – see section 5.1 for further discussion.
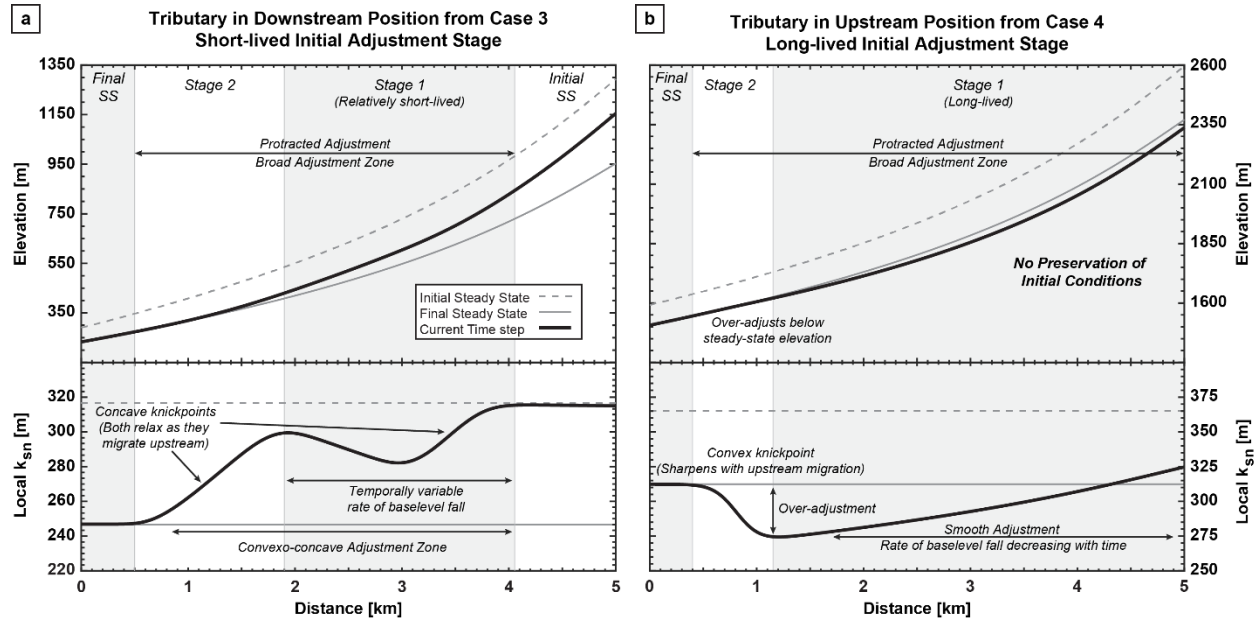
1151

1152

1153 **Figure 8.** Representative examples of multi-stage tributary response in Cases 3 (a) & 4 (b). Note,
1154 upstream positions always experience relatively longer initial adjustment stages than downstream
1155 positions, regardless of rainfall gradient. Grey shaded and white regions show where initial and final
1156 steady states (SS) and different adjustment stages are represented along the profile lengths, as indicated
1157 across top axis. a) Shows a tributary located in a relatively downstream position, 15 km from trunk outlet
1158 ($x < x_{sc}$) and 300 kyr into transient adjustment of the catchment in Case 3, where the initial adjustment
1159 stage is relatively short-lived. Despite this, protracted adjustment creates a several-kilometer-wide
1160 adjustment zone with relatively smooth but notable along-stream variations in k_{sn}. This pattern is subtle
1161 on the longitudinal profile. b) Shows a tributary located in an upstream position, 45 km from the trunk
1162 outlet ($x > x_{sc}$) and 1.725 Myr into transient adjustment of the catchment in Case 4, where the initial
1163 adjustment stage is long-lived. The initial adjustment stage reshapes the entire profile prior to adjustment
1164 of the trunk profile, but no transient knickpoints or other obvious topographic indicators of such
1165 significant modification are present, with smoothly varying local k_{sn} values within 10% of the mean. Also,
1166 note overadjustment means that the increase in channel steepness required to reach steady state contrasts
1167 with net reduction in channel steepness during transient adjustment.
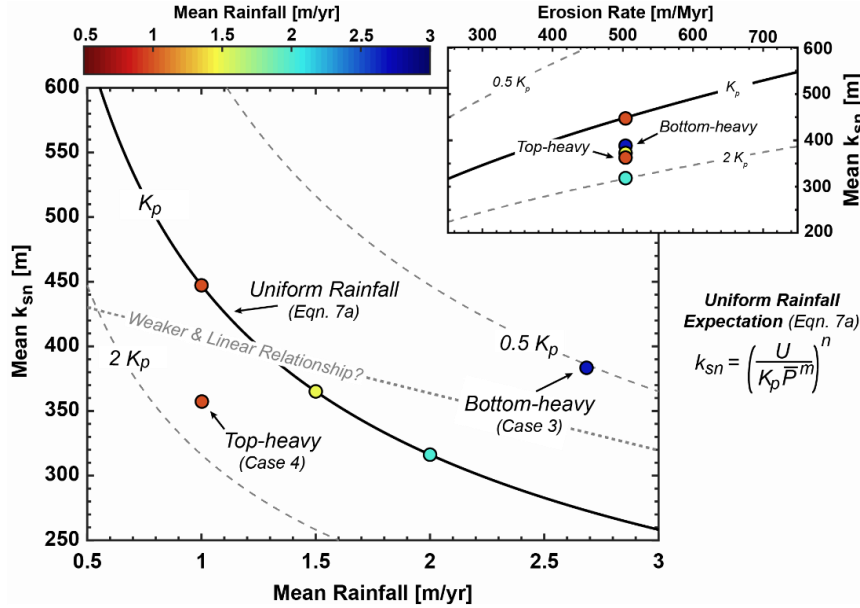
1168

Figure 9. Plot illustrating how rainfall gradients systematically influence correlation between mean rainfall and k_{sn} at steady state, and consequences for relationship between channel steepness and erosion rate (inset). A common symbology is used in both the main figure and the inset. Expected SPM relationship based on uniform climate (uniform erosional efficiency, K) from equation 7a is shown in solid back line. Grey long-dashed lines represent changes in $K = K_p P^m$ by factors of two, which correspond to uniform changes in mean rainfall and erosional efficiency of the same magnitude ($m = 1$). Circles colored by mean rainfall reflect scenarios shown in Figure 1 – uniform rainfall of 1, 1.5, and 2 m/yr, and top- and bottom-heavy gradients (labeled as Case 4 and Case 3). While K_p is uniform in all scenarios, rainfall gradients cause dispersion (apparent differences in erosional efficiency) from the expected relationship (solid black line) equivalent to differences in K_p of approximately a factor of two (inset). For instance, the bottom-heavy case where mean rainfall is ~2.7 m/yr exhibits an apparent ~50% reduction in erosional efficiency based on mean k_{sn} (plots on $K \approx 0.5 K_p$ curve in main figure) and thus plots where one would expect a catchment that experiences half as much rainfall to plot in the inset. Dotted line in main figure illustrates, conceptually, how this dispersion could distort inferred relationships between mean rainfall and channel steepness (weaker and quasi-linear in this case), even at steady state and in systems where the SPM is a complete description of the controls on channel profile form. Where uplift rates are unknown, this systematic bias in apparent erosional efficiency due to rainfall gradients is a potential source of dispersion in relationships between k_{sn} and erosion rate (inset), which in and of itself can obscure or distort the importance of variations in rainfall on channel steepness and erosion rates.
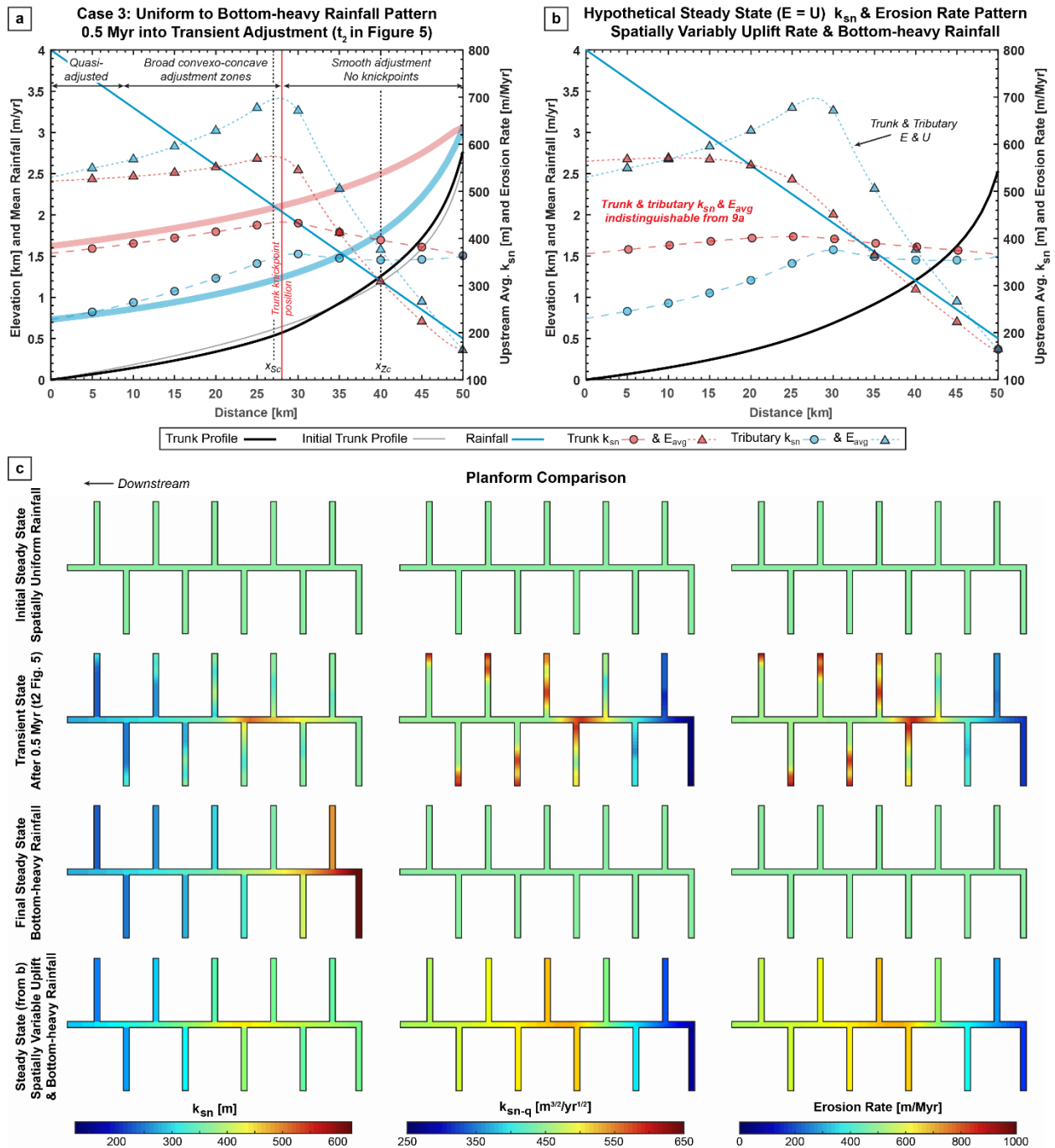
1188

Figure 10. Illustration of potentially misleading spatial patterns that arise among channel steepness, rainfall, and erosion rates during transient adjustment to a change in rainfall pattern, particularly when erosion rate and morphometrics are averaged at catchment scale as is common – see section 5.1.2 for detailed discussion. a) Shows time slice at 0.5 Myr into transient adjustment of Case 3 (t_2 in Figure 5). For clarity, a subsample of ten data points is shown for each model dataset; connecting dashed line is populated from full model. Thick colored bands (red for trunk stream, blue for tributaries) show final steady state upstream-averaged k_{sn} pattern toward which the modelled landscape is adjusting. Position of

1197   trunk knickpoint, defined as upstream extent of quasi-steady state adjustment, is shown by red solid line
1198   (compares with panel c). Zones describing morphological characteristics of tributary catchments are
1199   shown across the top axis (compare with panel c). b) Modelled steady state k_{sn} and erosion rate pattern of
1200   a catchment experiencing a bottom-heavy rainfall gradient and a spatial gradient in uplift rate that
1201   matches the catchment-averaged tributary erosion rates in panel a). c) Shows planform development of
1202   local k_{sn}, k_{sn-q}, and erosion rates at initial and final steady states, a transient time slice from Case 3, and
1203   steady state pattern from (b). Downstream is to the left, as indicated. Transient time slice and tributaries
1204   are the same as in panels (a & b). Note that trunk and tributary profiles are not illustrated to scale (Table
1205   1). Importantly, we note here that while catchment-mean data (and arguably along-stream k_{sn}) can be
1206   indistinguishable between the transient and spatial uplift gradient scenarios, the expected patterns of
1207   erosion rate and k_{sn-q} are distinct.